

Measuring the fine structure constant on a white dwarf surface; a detailed analysis of Fe V absorption in G191-B2B

J. Hu^{1*}, J. K. Webb^{2†}, T. R. Ayres³, M. B. Bainbridge⁴, J. D. Barrow⁵,
 M. A. Barstow⁴, J. C. Berengut², R. F. Carswell⁶, V. Dumont⁷, V. Dzuba²,
 V. V. Flambaum², C. C. Lee⁵, N. Reindl⁸, S. P. Preval⁴, W.-Ü L. Tchang-Brillet⁹.

¹ADACS, Swinburne University of Technology, Hawthorn, VIC 3122, Australia

²School of Physics, University of New South Wales, Sydney, NSW 2052, Australia

³Center for Astrophysics and Space Astronomy, University of Colorado, 389 UCB, Boulder, Colorado 80309-0389, USA

⁴Department of Physics and Astronomy, University of Leicester, University Road, Leicester LE1 7RH, UK

⁵DAMTP, Centre for Mathematical Sciences, University of Cambridge, Cambridge CB3 0WA, UK

⁶Institute of Astronomy, Madingley Road, Cambridge CB3 0HA, UK

⁷Computational Research Division, Lawrence Berkeley National Laboratory, Berkeley, CA 94720, USA

⁸Institute for Physics and Astronomy, University of Potsdam, Karl-Liebknecht-Str. 24/25 14476 Potsdam, Germany

⁹LERMA, Observatoire de Paris-Meudon, PSL Research University, CNRS UMR8112, Sorbonne Université, F-92195 Meudon, France

Received XXX. Accepted YYY.

ABSTRACT

The gravitational potential $\phi = GM/Rc^2$ at the surface of the white dwarf G191-B2B is 10,000 times stronger than that at the Earth's surface. Numerous photospheric absorption features are detected, making this a suitable environment to test theories in which the fundamental constants depend on gravity. We have measured the fine structure constant, α , at the white dwarf surface, used a newly calibrated Hubble Space Telescope STIS spectrum of G191-B2B, two new independent sets of laboratory Fe V wavelengths, and new atomic calculations of the sensitivity parameters that quantify Fe V wavelength dependency on α . The two results obtained are: $\Delta\alpha/\alpha_0 = 6.36 \pm (0.33_{\text{stat}} + 1.94_{\text{sys}}) \times 10^{-5}$ and $\Delta\alpha/\alpha_0 = 4.21 \pm (0.47_{\text{stat}} + 2.35_{\text{sys}}) \times 10^{-5}$. The measurements hint that the fine structure constant increases slightly in the presence of strong gravitational fields. A comprehensive search for systematic errors is summarised, including possible effects from line misidentifications, line blending, stratification of the white dwarf atmosphere, the quadratic Zeeman effect and electric field effects, photospheric velocity flows, long-range wavelength distortions in the HST spectrum, and variations in the relative Fe isotopic abundances. None fully account for the observed deviation but the systematic uncertainties are heavily dominated by laboratory wavelength measurement precision.

Key words: White Dwarfs; Gravitation; Atomic processes

1 INTRODUCTION

General relativity has passed all weak-field observational and experimental tests to date. Nevertheless, the theory predicts singularities on small scales and is incompatible with quantum field theory. To be compatible with cosmological observations, the theory also requires most of the energy content of the universe to be in the form of an unknown dark energy. These things lead us to expect that GR will ultimately

become the low-energy limit of some future more fundamental unification theory. Searches for departures from standard GR, particularly in stronger-field situations, are important in this respect. This is the aim of the work described in this paper.

Fundamental constants may vary in the presence of strong gravitational fields, a possibility first proposed by Dicke (1959, 1964), the latter republished in Dicke (2019), with a related discussion given in Bekenstein (1982). More recent ideas concerning quantum gravity unification theories allow the possibility of space and time variations in the low-energy ‘constants’ of Nature, either because of the presence

*Email: jitinghu@swin.edu.au

†Email: jkw@phys.unsw.edu.au

of extra space dimensions or the non-uniqueness of the quantum vacuum state for the universe, e.g. Uzan (2011). Strong-field tests using pulsar timing observations in a triple stellar system place tight constraints on departures from standard General Relativity (Archibald et al. 2018; Voisin et al. 2020).

Since the gravitational potential at the surface of a white dwarf is typically 4 to 5 orders of magnitude stronger than on Earth, white dwarf atmospheres provide an interesting environment to search for new physics or new tests of the weak equivalence principle. Discussions concerning relativistic effects in white dwarfs include Wheeler et al. (1968); Jain et al. (2016); Carvalho et al. (2018). If relativistic effects are weak (as is the case for white dwarf surfaces; $GM/Rc^2 \sim 10^{-4}$, within an order of magnitude of the gravitational potential perturbation observed on the last scattering surface of the microwave background), the total scalar charge is proportional to the number of nucleons in the object Flambaum & Shuryak (2008).

Near massive gravitating bodies, different types of couplings between scalar fields and other fields can lead to an increase or decrease in the coupling constant strengths Magueijo et al. (2002). These scalar fields can be the carriers of variations in traditional constants of physics, like G , α and m_e/m_p and so precision studies of white dwarf atmospheres offers a new laboratory for fundamental physics that is not available on Earth. For small variations, the scalar field variation is proportional to the change in the dimensionless gravitational potential, $\phi = GM/Rc^2$ and hence to the compactness (M/R) of an object. Compact objects with high mass and small radius, could thus exhibit variations in the fine structure ‘constant’, α , for example, with a relative change given by

$$\frac{\Delta\alpha}{\alpha_0} = \frac{\alpha_\phi - \alpha_0}{\alpha_0} \propto \Delta\phi, \quad (1)$$

where $\Delta\phi$ is a change in the gravitational potential (in this case the difference between the white dwarf and terrestrial values). Inhomogeneous variations in the cosmological setting were studied in Barrow et al. (2002); Mota & Barrow (2004a,b); Barrow & Mota (2003).

In this paper, we present a detailed analysis of the spectrum of G191-B2B to measure $\Delta\alpha/\alpha_0$. The first such analysis was reported in Berengut et al. (2013). Both that paper and this make use of the *Many Multiplet method* (Dzuba et al. 1999b; Webb et al. 1999; Dzuba et al. 2003; Flambaum & Dzuba 2009). However, a new analysis of G191-B2B is required because: (i) two new samples of Fe V laboratory wavelength measurements have since been published, (ii) the G191-B2B HST STIS spectra themselves have been refined/re-reduced, in principle providing a more accurate calibration, (iii) the Berengut et al. (2013) analysis used simple line centroid measurements, which do not readily identify line blends or other anomalies. Here we use a different approach – simultaneously fitting many Fe V transitions using Voigt profiles (which effectively means that we model the data using far fewer positional parameters), and (iv) the coefficients used to parameterise each transition’s sensitivity to a change in α have been independently re-calculated (Section 4.3). Having 2 independent sets yields an approximation for associated uncertainties.

The structure of the remainder of this paper is as follows: Section 2 provides a brief reminder of basic white dwarf

astrophysics and describes previous constraints. Section 3 describes the HST/STIS spectra of the white dwarf G191-B2B. Section 4 details all atomic/laboratory data used. Section 5 discusses line detection in the G191-B2B spectrum, matching those lines with the laboratory Fe V wavelengths, and the further refinement of the sample to remove weak and asymmetric features. Section 6 presents the modelling procedures for measuring $\Delta\alpha/\alpha_0$ and Section 7 summarises the results of numerical calculations quantifying several possible sources of systematic error.

Sections 8 and 9 present and discuss the final results.

2 OBSERVATIONAL CONSTRAINTS USING WHITE DWARFS

White dwarfs are the most common end-products of stars. More than 95% of stars in our Galaxy will end up as white dwarfs. Stars with initial masses of $\sim(1-8) M_\odot$ eventually evolve into white dwarfs (Fontaine et al. 2013). As stars evolve, the energy generated by nuclear interactions fails to balance gravity and collapse occurs. Stable radii are reached when electron degeneracy pressure balances gravity (Koester & Chanmugam 1990), leaving very compact, high surface gravity remnants, white dwarfs. A typical white dwarf has an oxygen/carbon core surrounded by a thin hydrogen/helium (H/He) envelope. Due to processes such as levitation (Chayer et al. 1995) and debris accretion from disrupted planetary systems, interstellar material, or comets (Zuckerman et al. 2003), metallic elements are found in the atmosphere.

White dwarfs are classified according to spectral features (e.g. atmospheric composition and colour), DA white dwarfs being those with a hydrogen enriched atmosphere (Sion et al. 1983). These white dwarfs are useful test-beds for investigating dependence of fine-structure constant variation on strong gravitational field. Some non-DA white dwarfs that have similar characteristics can also be used, such as the hot sub-dwarf O star, BD+28°4211. White dwarf characteristics that are desirable for α measurements include (i) a strong surface gravitational field; DA white dwarfs can have surface gravity $\log g$ between ~ 7 and ~ 8 (Bergeron et al. 1992), and (ii) multiple heavy element transitions; various species, including Fe V or Ni V have been observed in white dwarf spectra (Sion et al. 1992; Holberg et al. 1994; Werner & Dreizler 1994). These highly ionised lines are particularly useful for measuring variation in fine-structure constant (α), as they are very sensitive to a change in α .

Hot DA white dwarfs with metal lines typically have effective temperatures $T_{\text{eff}} \geq 50,000$ K (Barstow et al. 2003, 2014). The *Space Telescope Imaging Spectrograph (STIS)* provides the highest resolution available for UV spectroscopy, the E140H grating having a resolving power of 114,000. Detailed analyses of the white dwarf G191-B2B are reported in Preval et al. (2013); Rauch et al. (2013). By comparing the observed data with NLTE model spectra, many Fe V and Ni V absorption features were identified.

The first astronomical measurement of α variation in strong gravitational fields (Berengut et al. 2013) used the Preval et al. (2013) spectrum and line identifications. Applying the many-multiplet method (Dzuba et al. 1999b; Webb et al. 1999), two $\Delta\alpha/\alpha_0$ measurements using Fe V and Ni

V lines separately gave $\Delta\alpha/\alpha_0(\text{Fe V}) = (4.2 \pm 1.6) \times 10^{-5}$, and $\Delta\alpha/\alpha_0(\text{Ni V}) = (-6.1 \pm 5.8) \times 10^{-5}$. The discrepancy between these two measurements suggested significant laboratory wavelength systematics in either the Fe V or the Ni V line lists, or both.

Analyses of additional spectra are described in Bainbridge et al. (2017a,b), who discuss the possibility of making $\Delta\alpha/\alpha_0$ measurements over a wide range in surface gravity using 8 white dwarfs, including G191-B2B. Collectively, the 8 results based on Fe V hint at a non-zero (positive) $\Delta\alpha/\alpha_0$ and a possible correlation with field strength. However, since those measurements are highly preliminary and include no estimate of systematics, we defer any further quantitative comments regarding those spectra to a later paper.

3 ASTRONOMICAL DATA

The analysis described in this paper is based on a high signal to noise STIS FUV spectrum of the white dwarf G191-B2B. The observations, data reduction, and other details are described fully in Hu et al. (2019), so only a brief summary is given here. G191-B2B is a common calibration source for STIS so the total integration time is high. In total, 37 archival E140H exposures of G191-B2B using the $0.2 \times 0.2''$ aperture were used. The E140H observations were conducted between 1998 and 2009 in observing cycles 7, 8, 10, and 17. The total E140H exposure time is 17.36 hours. In addition to the E140H exposures, which cover the wavelength range (1150–1700) Å. There are also 5 exposures taken between 2000 and 2009 in observing cycles 9, 10 and 17, using the shortest wavelength setting (1763 Å) with the E230H grating covering the range (1630–1897) Å. The full coverage of the spectrum spans 1150 Å to 1897 Å. The spectral resolution is $\lambda/\Delta\lambda \approx 114,000$.

4 ATOMIC DATA

4.1 Laboratory & Ritz wavelengths

The analysis of G191-B2B by Berengut et al. (2013) showed that wavelength errors dominate the $\Delta\alpha/\alpha_0$ uncertainty. That analysis used the best available wavelengths at that time (Ekberg 1975). Two more new Fe V wavelength datasets have been published since then: the Ritz calculations of Kramida (2014), and the laboratory measurements by Ward et al. (2019) at NIST. For the measurement of $\Delta\alpha/\alpha_0$ presented in this paper, we used the Fe V electric dipole (E1) transitions available from these two new wavelength datasets (the majority being $3d^34s$ - $3d^34p$ transitions) that lie in the range 1149 Å to 1705 Å. We now comment briefly on each set of Fe V laboratory wavelengths used in our analysis.

Kramida 2014 (hereafter, K14):

This set of Fe V lines is from Kramida (2014). He used previous laboratory measurements of around 2000 wavelengths, including Ekberg (1975), Azarov et al. (2001), Fawcett & Henrichs (1974), Kalinin et al. (1985), with the lines in the wavelength range of interest to this study being dominated by the measurements of Ekberg (1975). Kramida

(2014) applied a least squares fitting method (Kramida 2011) to determine optimised energy levels and hence Ritz wavelengths. Since multiple spectral lines are used to determine the energy levels, Ritz wavelengths generally have smaller uncertainties than individual laboratory experiment sets. However, this also means that wavelength calibration errors affect the Ritz wavelengths in a complex way as they are determined from spectral lines in different wavelength regions. Within our wavelength range of interest, the uncertainties lie in the range is 1.5 to 8 mÅ.

Ward et al 2019 (hereafter, W19):

This set of Fe V lines comes from an experiment to measure Fe V and other species at the National Institute of Standards and Technology, Gaithersburg, Maryland USA (Ward & Nave 2015a,b; Ward et al. 2019). The experiment measured 164 Fe V lines between 1200 Å and 1600 Å. In this sample, uncertainties are assigned to each Fe V wavelength and lie in the range 2.4 to 10 mÅ.

We opt to remove the least accurate Fe V wavelengths from both samples. For K14 we discard all lines with uncertainties greater than 4 mÅ. The 4 mÅ cut is mildly arbitrary but was chosen because it is the measurement uncertainty for the Fe V sample from Ekberg (1975) on which the optimised K14 sample is based and in order retain a significant number lines in the sample. This leaves 377 lines. For W19, we do the same (but see the caption to Table A1). This leaves 129 lines.

To examine consistency, in Figure 1 we plot wavelength difference for pairs of lines from the two wavelength datasets. $\Delta\lambda$, the difference between W19 and K14 wavelength, has a mean value of 0.2 mÅ, with a standard deviation of 3.7 mÅ.

4.2 Other atomic data

Since we are fitting Voigt profiles to the observed Fe V absorption lines in the G191-B2B atmosphere, the column density parameter returned from the Voigt profile fitting is only a measure of line strength (and does not give a true column density estimate). To calculate Voigt profile models, we necessarily require values for the oscillator strength f and damping constant Γ . The f values are taken from Kramida (2014), supplemented by 18 missing values from the Kurucz database¹. Γ values are taken from Aggarwal et al. (2017) where available and Kurucz's values used otherwise. However, in our modelling procedure, each observed transition is assigned its own column density and velocity dispersion parameter (b -parameter). Only relative line positions are tied in the fitting procedure. This means that the oscillator strengths and damping coefficients are effectively treated as free parameters.

4.3 Sensitivity coefficient calculations

The wavenumber ω of a transition measured in the white dwarf rest-frame is given by

$$\omega = \omega_0 + qx, \quad (2)$$

¹ <http://kurucz.harvard.edu/>

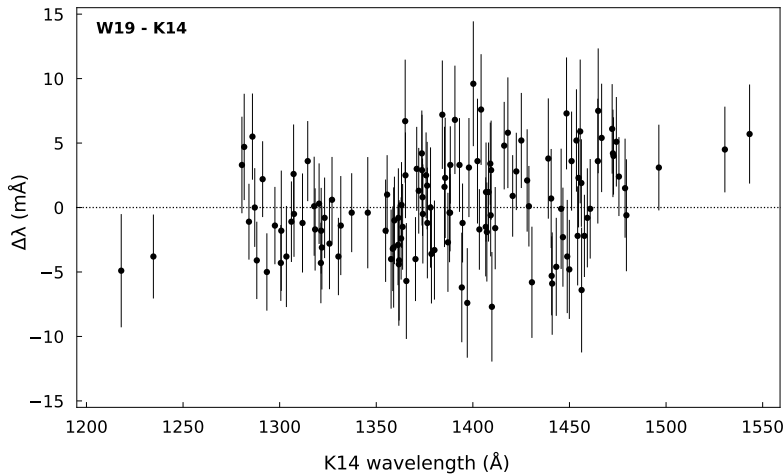


Figure 1. The difference between the W19 and K14 wavelengths. See Ward et al. (2019) for a detailed comparison between Fe V wavelength sets.

where ω_0 is the laboratory wavenumber, q is the sensitivity coefficient to changes in α , and $x = (\alpha_\phi/\alpha_0)^2 - 1$ (Dzuba et al. 1999a; Webb et al. 1999).

New Fe V q -coefficients for transitions involving $3d^34s$ and $3d^34p$ configurations have been calculated. The same approach as in Ong et al. (2013) has been followed, but the new calculations include about a hundred new states, leading to an enormous number of new electric dipole transitions. The calculations use the combined configuration interaction and the many body perturbation theory method, CI+MBPT (Dzuba et al. 1996; Dzuba & Johnson 1998). The B-spline technique (Johnson & Sapirstein 1986) is used to construct a single-electron basis set. The calculations are done in the V^{N-4} approximation (Dzuba 2005), which means that the initial self-consistent Hartree-Fock procedure is done for the closed-shell Ar-like Fe IX ion with all four valence electrons removed. The basis states in valence space are calculated in the frozen field of the Ar-like Fe IX core. The CI technique is used to construct four-electron valence states while MBPT is used to include core-valence correlations (see Ong et al. (2013); Dzuba et al. (1996); Dzuba & Johnson (1998) for further details).

An analysis of the accuracy of the calculations is described in Ong et al. (2013). This includes calculations with different initial approximations (V^N , V^{N-1} , etc.) which give very close results. Therefore, in the present paper we use just one approach based on the V^{N-4} potential. It is slightly different from the methods used in Ong et al. (2013) and independent computer codes were used. Comparing the two sets of coefficients therefore provides an empirical estimate of the q -coefficient uncertainties. In the end, we believe that the q -coefficient uncertainty does not exceed 10%. For Fe V lines to be used in measuring $\Delta\alpha/\alpha_0$, we must of course have q -coefficients; 345 of the 377 in the K14 sample and 120 of the 129 in the W19 sample have these.

Inspection of Table A1 shows that some transitions have not been assigned q -coefficients. The reason for this is that due to the high density of excited states, matching the observed and calculated energy levels is sometimes ambiguous.

This means we cannot reliably assign q -coefficients to some of the observed transitions. Therefore, we have not presented values of q in some cases. We noted (subsequent to the completion of this work) that matching energy levels can be clarified using the procedures of Kramida (2013). This is a possible area to be developed in future work so that more transitions can be used.

5 LINE DETECTION, IDENTIFICATION, AND SAMPLE REFINEMENT

5.1 5σ detections using RDGEN

RDGEN is a multi-purpose program for spectroscopic data analysis (Carswell et al. 2014). One useful function is the detection of absorption lines above a given statistical significance, relative to a user-supplied continuum level. A reliable spectral variance array is required. The algorithm uses the known spectral resolution to constrain the minimum separation between adjacent or blended features. It returns line centroids, equivalent widths, and other relevant measurements, with associated error estimates. Our first step is to measure lines in the G191-B2B spectrum above a 5σ detection threshold.

5.2 Matching the detected and laboratory wavelengths

The laboratory wavelength sets are derived from terrestrial experiments for which $\Delta\alpha/\alpha_0 = 0$. The number of absorption lines per unit wavelength interval in the spectrum of G191-B2B is reasonably high, so it may be possible to wrongly associate observed and laboratory lines if the tolerance is insufficiently stringent and/or if in fact $\Delta\alpha/\alpha_0 \neq 0$ near a white dwarf. If $\Delta\alpha/\alpha_0 \neq 0$ near a white dwarf, making the assumption that $\Delta\alpha/\alpha_0 = 0$ may result in line misidentifications (and bias a $\Delta\alpha/\alpha_0$ measurement towards zero). Since we do not know *a priori* the value of $\Delta\alpha/\alpha_0$ at the white dwarf atmosphere, it is therefore preferable to avoid making

ID	C1	T1	J1	C2	T2	J2	E1 (cm ⁻¹)	E2 (cm ⁻¹)	K14		W19		f	Γ (s ⁻¹)	q (cm ⁻¹)
									λ (Å)	$\delta\lambda$ (Å)	λ (Å)	$\delta\lambda$ (Å)			
60	3d3.(2D1).4s	3D	1	3d3.(2D1).4p	3P*	1	258769.6	335267.9	1307.2190	0.0030	1307.2216	0.0024	9.6e-02	4.17E+09	2862
61	3d3.(2P).4s	1P	1	3d3.(2P).4p	1P*	1	219486.7	295973.0	1307.4242	★ 0.0023	1307.4237	◇ 0.0024	2.2e-01	6.80E+09	2311
62	3d3.(2G).4s	3G	4	3d3.(2P).4p	3D*	3	209109.9	285474.0	1309.5147	0.0020			1.1e-02	5.65E+09	2992
63	3d3.(2P).4s	3P	1	3d3.(2D2).4p	3P*	0	214611.3	290903.4	1310.7510	0.0030			6.0e-04	8.06E+09	3286
64	3d3.(4P).4s	3P	2	3d3.(2D2).4p	3D*	3	213649.0	289912.8	1311.2378	0.0019	1311.2293	0.0074	3.8e-02	5.88E+09	2389
65	3d3.(2P).4s	1P	1	3d3.(2D2).4p	1D*	2	219486.7	295716.2	1311.8290	★ 0.0030	1311.8278	◇ 0.0024	1.9e-01	1.01E+10	1616
66	3d3.(4P).4s	3P	0	3d3.(2D2).4p	3D*	1	212542.0	288669.5	1313.5851	★ 0.0023			6.6e-02	6.17E+09	2507
67	3d3.(2G).4s	3G	3	3d3.(2P).4p	3D*	2	208838.0	284911.0	1314.5256	★ 0.0017	1314.5292	◇ 0.0026	2.2e-03	5.21E+09	2920
68	3d3.(2D1).4s	3D	2	3d3.(2D1).4p	3P*	2	258628.6	334509.2	1317.8610	0.0030	1317.8611	0.0024	7.0e-02	4.20E+09	
69	3d3.(2G).4s	3G	3	3d3.(2H).4p	3H*	4	208838.0	284690.3	1318.3505	0.0021	1318.3488	0.0024	6.0e-02	5.99E+09	3660

Table 1: Summary of atomic data. K14 are Ritz wavelengths (Kramida 2014). Lines that we used for measuring $\Delta\alpha/\alpha_0$ are marked with a ★. The bulk of the analysis described in this paper was carried out on a pre-publication version of the W19 tabulated FeV lines that had been assigned different uncertainty estimates. The initial cut (accepting only lines with uncertainties ≤ 4 mÅ), and the subsequent filtering, results in our final W19 sample being those lines marked in this table with a ◇. The pre-publication FeV tabulation has not been given here – in this table we list the W19 data as published in Ward et al. (2019). Columns 2-4 and 5-7 are the lower and upper level configuration, term, and J values, adopted from Table 1 in Kramida (2014) and from NIST (https://physics.nist.gov/PhysRefData/ASD/lines_form.html). Columns 8 and 9 are the lower and upper energy levels. Oscillator strength f are from Kramida (2014) if available. 18 lines with missing values are supplemented by data from the Kurucz database (†). Γ values are taken from Aggarwal et al. (2017) where available. 15 lines with missing values are supplemented by data from Kurucz database (marked with a §). The q-coefficients given in this table are new calculations and supersede those of Ong et al. (2013). This table only shows 10 entries. The full table can be found in Table A1 in Appendix A1.

any assumption about $\Delta\alpha/\alpha_0$ when identifying the observed G191-B2B absorption lines. To avoid this problem, line identification is carried out as a function of $\Delta\alpha/\alpha_0$, over the range $-10^{-3} < \Delta\alpha/\alpha < 10^{-3}$, in steps of 10^{-5} . The K14 wavelengths have the largest number of lines available (345 lines) so this dataset was used for line identification.

The G191-B2B redshift used is obtained from the measured value of $v = 23.8 \pm 0.03$ km s⁻¹ (Preval et al. 2013), obtained using the weighted average of all the identified atmospheric lines (i.e. all identified species, not just Fe V).

Re-arranging Eq.2 and using $\omega = \omega'(1+z)$, the observed-frame laboratory wavelength becomes

$$\lambda' = \frac{\lambda_0(1+z)}{1+qx/\omega_0} \quad (3)$$

$$\approx \lambda_0(1+z) \left(1 - \frac{Q\Delta\alpha}{\alpha_0}\right), \quad (4)$$

where ω' is the observed-frame wavenumber, z is its redshift (the summed effects of stellar peculiar velocity and gravitational redshift), λ_0 is the terrestrial laboratory wavelength, the dimensionless quantity $Q=2q/\omega_0$, $x \approx 2\Delta\alpha/\alpha_0$, and where the first two Taylor series terms have been used to approximate the factor of $1/(1+qx/\omega_0)$ in Eq.3.

For a line to be identified as Fe V, we require the observed and laboratory wavelengths to agree within

$$\Delta\lambda = |\lambda_{\text{obs}} - \lambda'| \lesssim n\sqrt{\sigma(\lambda_{\text{obs}})^2 + \sigma(\lambda')^2}, \quad (5)$$

where λ_{obs} and λ' are the observed-frame white dwarf and laboratory wavelengths. The error contribution due to the white dwarf redshift is small compared to the other terms so has been ignored.

The results of these calculations for a range of n are illustrated in Figure 2. As can be seen, line identification maximises at or very close to $\Delta\alpha/\alpha_0 = 0$. The plateauing at large n occurs because the generous identification criterion results in many accepted identifications for each line. The

final tolerance used to select lines is $n = 3$. This procedure serves two purposes: first, it indicates that if $\Delta\alpha/\alpha_0$ does depart from zero, it is only by a small amount. Second, it suggests that even if we identify lines using $\Delta\alpha/\alpha_0 = 0$ with a 3σ tolerance, we are unlikely to bias the final result much.

5.3 Removing blended and weak lines

The total number of Fe V absorption lines detected in the G191-B2B spectrum using the above selection parameters was 199. We now refine this list by removing blended features. Where RDGEN detects multiple components in an absorption feature in the observed G191-B2B spectrum and where one of the detected components is Fe V and the other, or others, are not identified as Fe V, that whole absorption feature is discarded. This reduces the total number identified of Fe V lines to 164.

Another means of identifying blended profiles comes from the laboratory measurements. The K14 Fe V list identifies 8 cases where a line is resolved into 2 components on the basis of energy level calculations. These 8 lines are discarded, reducing the total number of identified Fe V lines to 148.

All remaining lines are fitted with Voigt profiles (convolved with the appropriate line spread function - see Section 6 for details). All line parameters are initially untied, i.e. each line is fitted with 3 parameters, column density, velocity dispersion parameter b , and redshift. χ^2 for each fit provides a check on goodness of fit. In a few cases, a high value of χ^2 indicates a non-Voigt line shape that had not been picked up earlier. Therefore these lines are removed from the analysis, discarding all lines that returned a $\chi_n^2 > 1.5$. This cut reduces the number of lines used from the G191-B2B spectrum from 148 to 135 lines.

Although lines have been detected above 5σ , some of the detected features are weak and do not contribute signif-

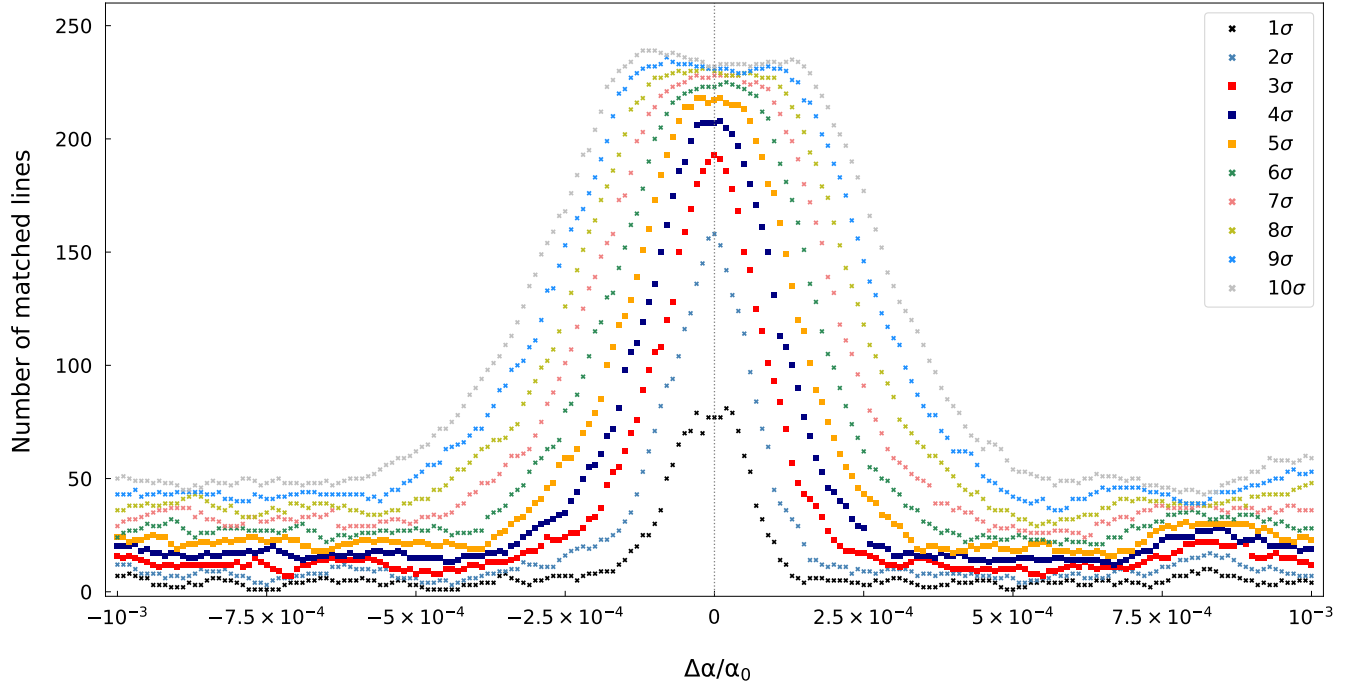


Figure 2. This figure illustrates the identification Fev lines in the spectrum of G191-B2B without assuming that $\Delta\alpha/\alpha = 0$, avoiding measurement bias. Lines are identified by stepping through $-10^{-3} < \Delta\alpha/\alpha < 10^{-3}$ in steps of 10^{-5} , modifying the Fev laboratory wavelengths according to Eq.3, then matching laboratory and rest-frame wavelengths using the tolerance defined by Eq.5. Each coloured curve corresponds to a different tolerance ($n = 1, 2, 3, \dots, 10$) for colours blue, green, grey, ..., red. As the identification criterion is relaxed, more lines are identified and the curves become increasingly flat-topped, as expected.

icantly to the $\Delta\alpha/\alpha_0$ measurement. For this reason we apply a final cut: lines with observed equivalent widths less than 0.002 \AA (38 lines) are removed. This step reduces the number of lines used from the G191-B2B spectrum from 135 to 97.

Finally, out of the 97 observed lines, all of which have K14 wavelengths, 63 also have W19 wavelengths.

6 MEASURING $\Delta\alpha/\alpha_0$

To solve for $\Delta\alpha/\alpha_0$, all Fe V redshift parameters are tied so that the whole sample is parameterised using one single redshift parameter. This removes 96 redshift parameters compared to the modelling described in Section 5.3. With all line redshifts tied, VPFIT is then used to solve for $\Delta\alpha/\alpha_0$. The default VPFIT set-up parameters (Carswell & Webb 2020a,b) are used with one important exception. The line spread function (lsf) of the spectrograph and grating (STIS with 140H) is non-Gaussian. Voigt profiles must be convolved with the appropriate lsf² during the modelling process. The non-default VPFIT set-up parameter is the number of sub-bins per pixel, which is set to 13, the number of pixels in the STIS lsf. The free parameters in the fit are thus *all* velocity dispersion parameters (one for each absorption line), *all* line strengths (“effective column densities”, one for each absorption line), one redshift parameter z for the whole sample, and one $\Delta\alpha/\alpha_0$ parameter.

² <http://www.stsci.edu/hst/instrumentation/stis/performance/spectral-resolution>

Once all redshift parameters are tied and the spectrum re-fitted, a small number of previously well-fitted lines produce high χ^2 values. Potential causes of this include:

- (i) Line blending that previously went undetected, i.e. an Fe V line may be correctly identified, but some other species is blended with it (the blended profile remaining reasonably symmetric and hence well-fitted by a single Voigt profile in Section 5.3) causing a small shift in the observed wavelength. These would only show up once tied redshifts were introduced;
- (ii) Wavelength calibration errors in the G191-B2B spectrum, although these would necessarily have to be localised, otherwise correlated groups of Fe V lines would appear discrepant and this seems not to be the case;
- (iii) Uncertainties in individual Fe V laboratory wavelengths;
- (iv) Incorrect q -coefficients could cause discrepant χ^2 values for individual lines (although if $\Delta\alpha/\alpha_0 = 0$, Eq.2 shows these have no effect);
- (v) It is possible (although unlikely) that misidentified lines remain in the sample, i.e. lines which have up until now been assumed to be Fe V but in fact are some other species.

Regardless of their origin, these points are clipped in an iterative procedure, removing individual spectral fitting regions having normalised $\chi_n > 2$ one at a time, re-fitting for $\Delta\alpha/\alpha_0$ at each iteration. There are a few groups of lines close to each other, thus in the same fitting region. In those cases, if $\chi_n > 2$ for the region as a whole, that region is discarded.

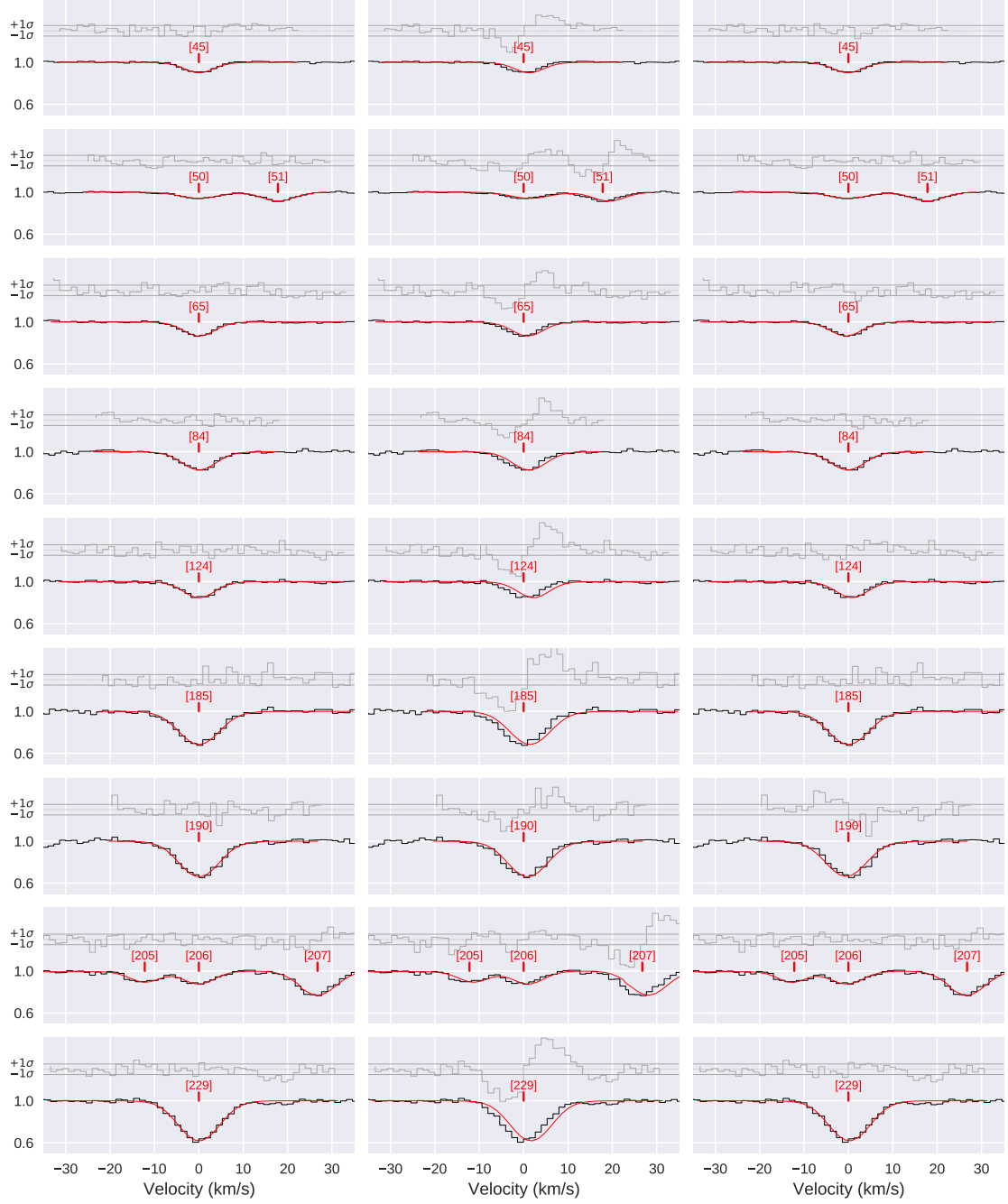


Figure 3. Examples of fits to Fe V lines in the G191-B2B E140 STIS spectrum using VPFIT. The x -axis is wavelength in Å and the y -axis is the normalised flux. The histogram is the data and the Voigt profile fits are over-plotted in red. The ticks indicate the line centres with wavelengths and line IDs (see Table A1). Normalised residuals are illustrated above each profile, the horizontal continuous lines indicate 1σ errors. The left hand column shows the best-fit model with $\Delta\alpha/\alpha_0$ as a free parameter. The middle column illustrates the exact same model as the left hand column but with $\Delta\alpha/\alpha_0$ reset to zero. The right hand column shows the best-fit model obtained when $\Delta\alpha/\alpha_0$ is fixed at zero.

After all selection procedures, the numbers of lines used for the two $\Delta\alpha/\alpha_0$ measurements are 92 with K14 wavelengths and 53 with W19 wavelengths.

7 MEASUREMENT UNCERTAINTIES

Known and potential sources of error have been investigated in considerable detail. Here we briefly described each one and list them in Table 3.

VPFIT measurement uncertainty: The VPFIT error (obtained from the covariance matrix at the best-fit solu-

ID	λ_{obs}	$\sigma(\lambda_{\text{obs}})$	EW	$\sigma(\text{EW})$	z [x10 ⁻⁵]	$\sigma(z)$ [x10 ⁻⁵]	b	$\sigma(b)$	logN	$\sigma(\log N)$	K14	W19
27	1250.833	0.001	0.003		7.88	0.06	4.99	0.30	12.12	0.02	✓	
36	1280.573	0.0012	0.00617	0.000197	8.17	0.04	5.36	0.18	13.22	0.01	✓	✓
38	1281.468	0.001	0.002		7.93	0.11	5.11	0.59	12.15	0.04	✓	
43	1286.015	0.001	0.002		7.73	0.06	3.68	0.30	12.51	0.02	✓	✓
45	1288.269	0.0009	0.00355	0.000148	7.89	0.04	3.98	0.20	12.73	0.01	✓	✓
48	1291.298	0.002	0.005		8.24	0.07	6.50	0.30	12.90	0.02	✓	✓
50	1293.409	0.001	0.003		7.85	0.06	5.47	0.27	13.09	0.02	✓	
51	1293.485	0.001	0.003		7.92	0.04	4.40	0.18	12.85	0.01	✓	
52	1297.651	0.001	0.005		7.95	0.04	5.13	0.17	12.91	0.01	✓	✓
53	1300.715	0.001	0.0047	0.000162	8.09	0.04	4.59	0.18	12.90	0.01	✓	

Table 2: Observed line wavelengths in the STIS spectrum of G191-B2B. ID refers to the number in column 1 of Table A1. λ_{obs} is the mean observed-frame wavelength of the absorption feature with uncertainty $\sigma(\lambda_{\text{obs}})$. EW is the equivalent width with uncertainty $\sigma(\text{EW})$. The absence of $\sigma(\text{EW})$ indicates that another line is nearby such that the detection algorithm interpreted the whole feature as a blend. Wavelength and equivalent widths are in Å. Columns 6-11 give redshift z, b-parameter (in km/s) and column density logN (N is in atoms/cm) with their associated uncertainties. A tick in the last two columns indicates that a line was used for measuring α . This table only shows 10 entries. The full table can be found in Table A2 in Appendix A1.

tion) depends only on the G191-B2B spectral properties and does not take into account other effects such as laboratory wavelength uncertainties. The method has been checked many times previously, e.g. King et al. (2009), but even so has been carefully verified again in this context. We generated 1000 synthetic spectra based on the Fe V laboratory wavelengths and the observed G191-B2B spectral properties. Each was fitted and the (known) $\Delta\alpha/\alpha_0$ solved for. The statistical distribution from the 1000 $\Delta\alpha/\alpha_0$ estimates can then be compared to the covariance matrix error estimate. The two values agree well.

Laboratory wavelength uncertainties: In the Fe V laboratory measurements made by Ekberg (1975), the nominal line wavelength uncertainties are given as 4 mÅ. As noted in Berengut et al. (2013), directly comparing the rest-frame G191-B2B and Ekberg wavelengths suggests the actual laboratory uncertainties were somewhat smaller.

Rather than a single uncertainty estimate, both the K14 and W19 Fe V tabulations provide a range of uncertainties, depending on line quality. For K14, the range for the Fe V lines used to measure $\Delta\alpha/\alpha_0$ here is 1.5 to 4 mÅ. For W19, the lines used to measure $\Delta\alpha/\alpha_0$ all have a nominal uncertainty of 3 mÅ.

Additional spectral simulations were therefore also done. First, a model of the white dwarf spectrum is created using the parameters derived from fitting the real spectrum. We perturb each Fe V laboratory wavelength randomly (using the published Fe V wavelength uncertainties) and then re-fit the spectrum using the modified laboratory wavelengths to re-measure $\Delta\alpha/\alpha_0$. The procedure is repeated 10,000 times for each set of laboratory wavelengths (K14 and W19), from which we can empirically determine the scatter in $\Delta\alpha/\alpha_0$ caused by Fe V laboratory wavelength uncertainties. The results of these numerical experiments also show the nominal K14 wavelength uncertainties are over-estimated although the nominal W19 uncertainties are close to correct.

Pt/Cr-Ne lamp and long-range wavelength distortion: The spectrum of G191-B2B used in this analysis is formed by combining 37 different exposures taken over an

11 year period. We do not know how stable the physical parameters of the HST on-board Pt/Cr-Ne emission-line calibration lamp were during time. The wavelength calibration can be also affected by (i) charge transfer inefficiency losses, (ii) instrumental changes such as thermal effects (heating and cooling of the optical bench), (iii) small variations of the position of the target along the spectrograph slit, and (iv) the HST orbital motion. All these factors must combine in some unknown way to produce a net wavelength calibration distortion.

Since there are no independent calibration sources for comparison, we parameterise any potential distortion using the method described in Dumont & Webb (2017). Following that procedure, we assume that the effects described above map to a linear distortion in velocity space. An additional free parameter (the velocity distortion slope) is included in the modelling that maps into a small shift on $\Delta\alpha/\alpha_0$ with an additional systematic error term, listed in Table 3.

Multiplet segregation: During the modelling procedure, although all line redshifts are tied such that the entire set of Fe V lines is fitted with one single redshift parameter, individual *b*-parameters are free. The reason for this is that there is evidence for stratification in the G191-B2B atmosphere (Barstow et al. 1999; Dreizler & Wolff 1999), which may imply that a single *b* value may not necessarily apply to all detected Fe V transitions. This is corroborated by a synthesised model atmosphere³ (Hubeny & Lanz 1995) for G191-B2B which predicts different atmospheric depths for different Fe V multiplets (also see Rauch et al. (2013)). The computation of synthetic spectra based on TLUSTY calculations are discussed in (Hubeny & Lanz 2011). Spatial segregation, in the presence of a velocity field that varies systematically with atmospheric depth, could in principle emulate varying α . Another consequence of Fe V multiplet segregation could be that different multiplets experience different gravitational redshifts. However, both of these effects have been modelled and both turn out to be very small. To illustrate this, using $\Delta z \approx GM\Delta r/r^2c^2$, assuming

³ <http://tlusty.oca.eu/>

a total photospheric height of 10km, the maximum gravitational redshift difference between absorptions created at the top and bottom of the atmosphere is $\Delta z \approx 10^{-8}$. This is an order of magnitude below the *statistical* measurement uncertainty on an individual line position, thus very small compared to the net uncertainty on $\Delta\alpha/\alpha_0$.

Fe isotopic abundances: The four stable Fe isotopes have terrestrial relative abundances ^{54}Fe (5.845%), ^{56}Fe (91.754%), ^{57}Fe (2.119%), ^{58}Fe (0.282%). Deviations from terrestrial abundances in the G191-B2B atmosphere will emulate small (energy level dependent) observed line shifts relative to a model based on terrestrial values. This may emulate a non-zero $\Delta\alpha/\alpha_0$. Variations from terrestrial isotopic abundances have been simulated by appropriately modifying the laboratory wavelengths and re-fitting to the G191-B2B spectrum to examine the impact on $\Delta\alpha/\alpha_0$.

Zeeman effects: If a magnetic field is present, the first order Zeeman effect would broaden or split the observed absorption lines. Two measurements of the magnetic field strength in G191-B2B, derived using independent methods give consistent results: [Bagnulo & Landstreet \(2018\)](#) find $B = -280 \pm 965$ G and ([Hu et al. 2019](#)) find $B < 2300$ G (3 σ upper limit). Using the latter, line shifts due to the quadratic Zeeman effect are $< 10^{-4}$ mÅ, four orders of magnitude below Fe V laboratory wavelength uncertainties. The quadratic Zeeman effect therefore has a negligible impact on measuring $\Delta\alpha/\alpha_0$ ([Hu et al. 2019](#)).

Electric field shifts: G191-B2B has a hydrogen rich atmosphere ([Holberg et al. 1991](#)). Example fundamental stellar parameters are provided by [Preval et al. \(2013\)](#) and [Barstow et al. \(2003\)](#): mass $0.52 M_\odot$, radius $0.0204 R_\odot$, and surface gravity $GM/R^2 = 3.4 \times 10^5$ m s $^{-2}$. Other measurements include those from [Rauch et al. \(2013\)](#) and [Gianninas et al. \(2011\)](#). At an effective temperature of 52,500K, a TLUSTY atmospheric synthesis model from [Preval et al. \(2013\)](#) gives a corresponding electron density of 7.0×10^{22} m $^{-3}$.

Although we may assume overall electrical neutrality, the proton-electron mass difference gives rise to a gravitational separation between the particles in the atmosphere. This separation in turn produces an opposing electric field. Equilibrium between the forces on protons and electrons gives

$$E \approx -\frac{m_p}{2e} \frac{GM}{R^2} \approx -1.8 \times 10^{-2} \text{ V/m} \quad (6)$$

([Alcock 1980](#); [Koester & Chanmugam 1990](#)). The quadratic electric field shift for atomic transitions is

$$\Delta\omega \sim \frac{-4\pi\epsilon_0 a_0^3 E^2}{\hbar c} \quad (7)$$

([Delone & Krainov 1999](#)) where $\omega (=v/c)$ is the wavenumber (as in Eq.2), a_0 is the Bohr radius, ϵ_0 is the permittivity of free space, and \hbar is the reduced Planck constant.

The corresponding shift $\Delta\omega$ is $\sim 10^{-18}$ cm $^{-1}$. Using Eq. 2, approximating $x = 2\Delta\alpha/\alpha_0$ so that $\Delta\alpha/\alpha_0 = \Delta\omega/q$, and using an illustrative $q = 1000$, we obtain $\Delta\alpha/\alpha_0 \sim 10^{-21}$. The electric field shift associated with a static electric field is thus negligible.

No.	Uncertainty	σ_α	Type
(1)	Statistical error	0.33, 0.47	R
(2)	Laboratory wavelength errors	1.59(3), 2.00(3)	S
(3)	Long-range distortion	0.1	S
(4)	Photosphere stratification - gravitational redshift effects	$\lesssim 0.1$	S
(5)	Photosphere stratification - bulk velocity flows	≤ 0.1	S
(6)	Fe isotopes - relative abundance variation	≤ 0.05	S
(7)	Zeeman effects	$\leq 10^{-5}$	S
(8)	Electric field shifts	Negligible	S

Table 3: Summary of actual and potential sources of random (R) and systematic (S) uncertainties and their magnitudes or upper limits. σ_α is the estimated uncertainty on $\Delta\alpha/\alpha_0$ in each case, in units of 10^{-5} . Where two entries appear, the first number corresponds to the results from the K14 Fe V wavelengths, the second from W19.

8 RESULTS

The final fine structure constant measurements at the G191-B2B surface, relative to the terrestrial value, are:

$$\Delta\alpha/\alpha_0(\text{K14, 92 lines}) = 6.36 \pm (0.33_{\text{stat}} + 1.94_{\text{sys}}) \times 10^{-5} \quad (8)$$

$$\Delta\alpha/\alpha_0(\text{W19, 53 lines}) = 4.21 \pm (0.47_{\text{stat}} + 2.35_{\text{sys}}) \times 10^{-5} \quad (9)$$

The systematic error contributions above are summed over all considered in Table 3, including upper limits. The K14 wavelengths produce a result that differs from a null result by 2.8σ whilst the W19 wavelengths indicate a 1.5σ effect. The error contributions are smaller for the K14 sample because of the larger number of Fe V lines in that sample.

Clearly, the approaches taken in the present paper are very different to the simpler analysis in [Berengut et al. \(2013\)](#), which gives $\Delta\alpha/\alpha_0 = 4.2 \pm 1.6 \times 10^{-5}$, where the uncertainty estimate is derived only from the nominal wavelength uncertainties of the best available Fe V wavelengths at that time ([Ekberg 1975](#)). In the present analysis we have used more recent independent Fe V laboratory measurements, and have explored and quantified a range of potential systematic errors. Our overall uncertainty remains dominated by laboratory wavelength errors, highlighting the need for more advanced calibration methods in laboratory experiments. Despite this, the agreement between all three results is striking.

9 DISCUSSION

In this paper, a comprehensive modelling procedure was applied to measure the fine structure constant at the surface of the white dwarf G191-B2B, using a single atomic species, Fe V. The *Many-Multiplet method* ([Dzuba et al. 1999a](#); [Webb et al. 1999](#)) has been used to search for any possible change in α in the presence of a gravitational potential 10,000 times the terrestrial value.

Wavelengths of Fe V from two laboratory datasets ([Kramida 2014](#); [Ward et al. 2019](#)), with improved uncertainties, were compared against the same transitions observed in the G191-B2B photosphere. Blended, weak, and asymmetric

absorption lines have been identified and removed from the sample to try and minimise associated systematic errors.

The overall scatter exhibited in Figure 1 is in good agreement with the estimated error bars. Nevertheless, Figure 1 suggests correlated deviations, so some systematic calibration problems may exist in one or both sets of new Fe V wavelengths. In the approximate wavelength range 1290–1360 Å, points lie on average below zero. Whilst the data appears reasonably symmetric about zero above 1350 Å, there is nevertheless a conspicuous clump of high points above ~1470 Å.

To advance this field further, several things are required: (i) it is imperative to improve laboratory wavelength precision by at least one order of magnitude, to ~ 0.1 mÅ or preferably much better, (ii) a large sample of white dwarf spectra should be analysed, and (iii) detailed analyses similar to that described in this paper should be carried out on other species such as FeIV or Ni V.

To summarise, the G191-B2B data calibration/reduction, the Fe V laboratory wavelengths, the q -coefficients, and the methodology used in this paper, are all different to those used in Berengut et al. (2013). Despite this, the consistency between that earlier result and this more detailed analysis is striking and hints (at the $\sim 3\sigma$ level) that perhaps the fine structure constant increases slightly in the presence of strong gravitational fields.

ACKNOWLEDGEMENTS

We are most grateful to G. Nave, A. Kramida, and J. Ward for extensive comments on a draft of this paper which lead to many improvements. JKW thanks the John Templeton Foundation, the Department of Applied Mathematics and Theoretical Physics and the Institute of Astronomy at Cambridge University for hospitality and support, and Clare Hall for a Visiting Fellowship during this work. JH is grateful for a CSC Fund and a UNSW scholarship. WULTB wishes to acknowledge support from the French CNRS-PNPS national program. MAB, JDB, MBB, SP and NR acknowledge the support of the Leverhulme Trust (Grant number 2015-278).

DATA AVAILABILITY

Based on observations made with the NASA/ESA Hubble Space Telescope, obtained from the data archive at the Space Telescope Science Institute. STScI is operated by the Association of Universities for Research in Astronomy, Inc. under NASA contract NAS 5-26555. The Hubble Space Telescope STIS spectra of G191-B2B are freely available in the Barbara A. Mikulski archive.

REFERENCES

- Aggarwal K., Bogdanovich P., Keenan F., Kisielius R., 2017, *Atomic Data and Nuclear Data Tables*, 114, 1
 Alcock C., 1980, *ApJ*, 242, 710
 Archibald A. M., et al., 2018, *Nature*, 559, 73
 Azarov V. I., Tchang-Brillet W.-U. L., Wyart J.-F., Launay F., Benharrouss M., 2001, *Physica Scripta*, 63, 438
 Bagnulo S., Landstreet J. D., 2018, *A&A*, 618, A113
 Bainbridge M., et al., 2017a, *Universe*, 3, 32
 Bainbridge M. B., et al., 2017b, in Tremblay P. E., Gaensicke B., Marsh T., eds, Astronomical Society of the Pacific Conference Series Vol. 509, 20th European White Dwarf Workshop. p. 375
 Barrow J. D., Mota D. F., 2003, *Classical and Quantum Gravity*, 20, 2045
 Barrow J. D., Magueijo J. a., Sandvik H. B., 2002, *Phys. Rev. D*, 66, 043515
 Barstow M. A., Hubeny I., Holberg J. B., 1999, *Monthly Notices of the Royal Astronomical Society*, 307, 884
 Barstow M. A., Good S. A., Holberg J. B., Hubeny I., Bannister N. P., Bruhwiler F. C., Burleigh M. R., Napiwotzki R., 2003, *MNRAS*, 341, 870
 Barstow M. A., Barstow J. K., Casewell S. L., Holberg J. B., Hubeny I., 2014, *MNRAS*, 440, 1607
 Bekenstein J. D., 1982, *Phys. Rev. D*, 25, 1527
 Berengut J. C., Flambaum V. V., Ong A., Webb J. K., Barrow J. D., Barstow M. A., Preval S. P., Holberg J. B., 2013, *Phys. Rev. Lett.*, 111, 010801
 Bergeron P., Saffer R. A., Liebert J., 1992, *ApJ*, 394, 228
 Bowen I. S., 1937, *Physical Review*, 52, 1153
 Carswell R. F., Webb J. K., 2020a, <https://people.ast.cam.ac.uk/~rfc/>
 Carswell R. F., Webb J. K., 2020b, <https://www.overleaf.com/read/vbxkcfnfgksr>
 Carswell R. F., Webb J. K., Cooke A. J., Irwin M. J., 2014, RDGEN: Routines for data handling, display, and adjusting, Astrophysics Source Code Library (ascl:1408.017), <https://www.ast.cam.ac.uk/~rfc/vpfit.html>
 Carvalho G. A., Marinho R. M., Malheiro M., 2018, *General Relativity and Gravitation*, 50
 Chayer P., Fontaine G., Wesemael F., 1995, *ApJS*, 99, 189
 Delone N. B., Krainov V. P., 1999, *Physics-Uspekhi*, 42, 669
 Dicke R. H., 1959, *Science*, 129, 621
 Dicke R. H., 1964, *The Theoretical Significance of Experimental Relativity*. New York: Gordon & Breach
 Dicke R. H., 2019, *General Relativity and Gravitation*, 51, 57
 Dreizler S., Wolff B., 1999, *A&A*, 348, 189
 Dumont V., Webb J. K., 2017, *MNRAS*, 468, 1568
 Dzuba V. A., 2005, *Phys. Rev. A*, 71, 032512
 Dzuba V. A., Johnson W. R., 1998, *Phys. Rev. A*, 57, 2459
 Dzuba V. A., Flambaum V. V., Kozlov M. G., 1996, *Phys. Rev. A*, 54, 3948
 Dzuba V. A., Flambaum V. V., Webb J. K., 1999a, *Phys. Rev. A*, 59, 230
 Dzuba V. A., Flambaum V. V., Webb J. K., 1999b, *Physical Review Letters*, 82, 888
 Dzuba V. A., Flambaum V. V., Marchenko M. V., 2003, *Phys. Rev. A*, 68, 022506
 Ekberg J. O., 1975, *Phys. Scr.*, 12, 42
 Fawcett B. C., Henrichs H. F., 1974, *A&AS*, 18, 157
 Flambaum V. V., Dzuba V. A., 2009, *Canadian Journal of Physics*, 87, 25
 Flambaum V. V., Shuryak E. V., 2008, in Danielewicz P., Piecuch P., Zelevinsky V., eds, American Institute of Physics Conference Series Vol. 995, Nuclei and Mesoscopic Physic - WNMP 2007. pp 1–11 ([arXiv:physics/0701220](https://arxiv.org/abs/physics/0701220)), doi:10.1063/1.2915601
 Fontaine G., Brassard P., Charpinet S., Randall S. K., Van Groo-

- tel V., 2013, in Shibahashi H., Lynas-Gray A. E., eds, Astronomical Society of the Pacific Conference Series Vol. 479, Progress in Physics of the Sun and Stars: A New Era in Helio- and Asteroseismology. p. 211
- Gianninas A., Bergeron P., Ruiz M. T., 2011, *ApJ*, **743**, 138
- Holberg J. B., Ali B., Carone T. E., Polidan R. S., 1991, *ApJ*, **375**, 716
- Holberg J. B., Hubeny I., Barstow M. A., Lanz T., Sion E. M., Tweedy R. W., 1994, *ApJ*, **425**, L105
- Hu J., et al., 2019, *MNRAS*, **485**, 5050
- Hubeny I., Lanz T., 1995, *ApJ*, **439**, 875
- Hubeny I., Lanz T., 2011, Synspec: General Spectrum Synthesis Program (ascl:1109.022)
- Jain R. K., Kouvaris C., Nielsen N. G., 2016, *Phys. Rev. Lett.*, **116**, 151103
- Johnson W. R., Sapirstein J., 1986, *Phys. Rev. Lett.*, **57**, 1126
- Kalinin S. K., Kononov E. Y., Perevertun V. M. e. a., 1985, "(Alma-Ata, USSR: Acad. Sci. Kazakh. SSR)"
- King J. A., Mortlock D. J., Webb J. K., Murphy M. T., 2009, *Mem. Soc. Astron. Italiana*, **80**, 864
- Koester D., Chanmugam G., 1990, Reports on Progress in Physics, **53**, 837
- Kramida A., 2011, *Computer Physics Communications*, **182**, 419
- Kramida A., 2013, *Fusion Science and Technology*, **63**, 313
- Kramida A., 2014, *ApJS*, **212**, 11
- Magueijo J., Barrow J. D., Sandvik H. B., 2002, *Physics Letters B*, **549**, 284
- Mota D. F., Barrow J. D., 2004a, *MNRAS*, **349**, 291
- Mota D. F., Barrow J. D., 2004b, *Physics Letters B*, **581**, 141
- Ong A., Berengut J. C., Flambaum V. V., 2013, *Phys. Rev. A*, **88**, 052517
- Preval S. P., Barstow M. A., Holberg J. B., Dickinson N. J., 2013, *MNRAS*, **436**, 659
- Rauch T., Werner K., Bohlin R., Kruk J. W., 2013, *A&A*, **560**, A106
- Sion E. M., Greenstein J. L., Landstreet J. D., Liebert J., Shipman H. L., Wegner G. A., 1983, *ApJ*, **269**, 253
- Sion E. M., Bohlin R. C., Tweedy R. W., Vauclair G. P., 1992, *ApJ*, **391**, L29
- Uzan J.-P., 2011, *Living Reviews in Relativity*, **14**, 2
- Voisin G., Cognard I., Freire P. C. C., Wex N., Guillemot L., Desvignes G., Kramer M., Theureau G., 2020, *A&A*, **638**, A24
- Ward J., Nave G., 2015a, IAU General Assembly, **22**, 2253006
- Ward J. W., Nave G., 2015b, in American Astronomical Society Meeting Abstracts #225. p. 339.03
- Ward J. W., Raassen A. J. J., Kramida A., Nave G., 2019, *ApJS*, **245**, 22
- Webb J. K., Flambaum V. V., Churchill C. W., Drinkwater M. J., Barrow J. D., 1999, *Physical Review Letters*, **82**, 884
- Werner K., Dreizler S., 1994, *A&A*, **286**, L31
- Wheeler J. C., Hansen C. J., Cox J. P., 1968, *Astrophys. Lett.*, **2**, 253
- Zuckerman B., Koester D., Reid I. N., Hünsch M., 2003, *ApJ*, **596**, 477

APPENDIX A: ATOMIC DATA**A1 Fe V wavelengths not used in this analysis**

In addition to the two Fe V laboratory wavelength sets used in this paper, Kramida (2014) (K14) and (Ward et al. 2019) (W19), there exist line lists from (at least) four previous Fe V laboratory experiments. An early Fe V study is by Bowen (1937), who identified 47 $3d^34s-3d^34p$ transitions (no quoted uncertainties but 10 mÅ implied). Fawcett & Henrichs (1974) and Kalinin et al. (1985) measured additional $3d^34s-3d^34p$ transitions not included in Ekberg's (Ekberg 1975) line list (measurement uncertainties (10 - 20 mÅ and 6 mÅ respectively). Azarov et al. (2001) find $3d^34p-3d^35s$ and $3d^34p-3d^34d$ transitions (6 mÅ uncertainties). These additional sources are noted here for completeness but were not used directly in our work.

Table A1: Summary of atomic data. K14 are Ritz wavelengths (Kramida 2014). Lines that we used for measuring $\Delta\alpha/\alpha_0$ are marked with a \star . The bulk of the analysis described in this paper was carried out on a pre-publication version of the W19 tabulated FeV lines that had been assigned different uncertainty estimates. The initial cut (accepting only lines with uncertainties ≤ 4 mÅ), and the subsequent filtering, results in our final W19 sample being those lines marked in this table with a \diamond . The pre-publication FeV tabulation has not been given here – in this table we list the W19 data as published in Ward et al. (2019). Columns 2-4 and 5-7 are the lower and upper level configuration, term, and J values for lower levels, adopted from Table 1 in Kramida (2014) and from NIST (https://physics.nist.gov/PhysRefData/ASD/lines_form.html). Columns 8 and 9 are the lower and upper level wavenumbers. Oscillator strength f are from Kramida (2014) if available. 18 lines with missing values are supplemented by data from the Kurucz database (\dagger). Γ values are taken from Aggarwal et al. (2017) where available. 15 lines with missing values are supplemented by data from Kurucz database (marked with a $\$$). The q -coefficients given in this table are new calculations and supersede those of Ong et al. (2013).

ID	C1	T1	J1	C2	T2	J2	E1 (cm ⁻¹)	E2 (cm ⁻¹)	K14		W19		f	Γ (s ⁻¹)	q (cm ⁻¹)	
									λ (Å)	$\delta\lambda$ (Å)	λ (Å)	$\delta\lambda$ (Å)				
0	3d3.(2D2).4s	1D	2	3d3.(2F).4p	1D*	2	220620.8	307644.0	1149.1179	0.0020			2.7e-02	4.78E+09	2143	
1	3d3.(2F).4p	3G*	5	3d3.(2H).4d	3G	5	307064.1	393894.9	1151.6660	0.0040			4.6e-02	8.32E+09 \dagger		
2	3d3.(2H).4p	3G*	4	3d3.(2G).4d	3G	5	292430.6	379110.4	1153.6720	0.0030			1.2e-02	1.23E+10 \dagger		
3	3d3.(2G).4p	3G*	5	3d3.(4F).4d	3F	4	280039.5	366564.3	1155.7380	0.0040			2.4e-02	1.18E+10 \dagger		
4	3d3.(2F).4p	3D*	1	3d3.(2H).4d	3F	2	308671.3	395049.7	1157.6970	0.0040			6.0e-02	1.15E+10 \dagger		
5	3d3.(2H).4p	3G*	4	3d3.(2G).4d	3G	4	292430.6	378763.2	1158.3120	0.0030			3.7e-03 \dagger	1.23E+10 \dagger		
6	3d3.(2H).4p	3G*	3	3d3.(2G).4d	3G	3	292513.1	378831.6	1158.5000	0.0030			1.0e-02 \dagger	1.29E+10 \dagger		
7	3d3.(2G).4p	3F*	4	3d3.(4F).4d	3F	4	280366.9	366564.3	1160.1280	0.0040			1.0e-02	1.12E+10 \dagger		
8	3d3.(2F).4p	3F*	4	3d3.(2D2).4d	3F	4	302602.3	388400.5	1165.5260	0.0030			1.0e-02	8.71E+09 \dagger		
9	3d3.(2G).4p	3F*	4	3d3.(4F).4d	3G	5	280366.9	366154.6	1165.6690	0.0050			1.8e-02	1.10E+10 \dagger		
10	3d3.(2G).4p	3F*	2	3d3.(4F).4d	3F	3	280539.6	366018.1	1169.8840	0.0030			6.0e-03	1.00E+10 \dagger		
11	3d3.(2G).4p	3G*	5	3d3.(4F).4d	3H	6	280039.5	365284.4	1173.0910	0.0040			2.2e-03 \dagger	1.18E+10 \dagger		
12	3d3.(2G).4p	3F*	3	3d3.(4F).4d	3F	3	280831.9	366018.1	1173.9000	0.0030			1.3e-02	1.10E+10 \dagger		
13	3d3.(2D1).4p	3F*	3	3d3.(2G).5s	3G	4	331367.3	415786.9	1184.5590	0.0050			3.0e-03	9.33E+09 \dagger		
14	3d3.(2G).4p	3F*	3	3d3.(4F).4d	3G	4	280831.9	365245.0	1184.6510	0.0040			2.0e-02	1.10E+10 \dagger		
15	3d3.(2G).4s	3G	3	3d3.(2H).4p	3G*	3	208838.0	292513.1	1195.0981	0.0016			1.0e-02	8.00E+09	3503	
16	3d3.(4P).4s	3P	0	3d3.(2P).4p	1P*	1	212542.0	295973.0	1198.5945	0.0020			5.0e-03	6.80E+09	4284	
17	3d3.(2G).4s	3G	4	3d3.(2H).4p	3G*	4	209109.9	292430.6	1200.1811	0.0017	1200.1951	0.0038	1.1e-02	7.75E+09	3155	
18	3d3.(2G).4s	3G	5	3d3.(2H).4p	1I*	6	209523.7	292365.6	1207.1183	0.0018			8.3e-05 \dagger	4.98E+09	2538	
19	3d3.(2G).4s	3G	5	3d3.(2H).4p	3G*	5	209523.7	292287.3	1208.2606	0.0015	1208.2472	0.0038	1.2e-02	8.20E+09	2890	
20	3d3.(4P).4s	3P	2	3d3.(2P).4p	1P*	1	213649.0	295973.0	1214.7130	0.0019			9.0e-03	6.80E+09	3027	
21	3d3.(4P).4s	3P	0	3d3.(4P).4p	3S*	1	212542.0	294643.9	1217.9973	0.0022	1217.9924	0.0038	5.9e-02	8.47E+09	3595	
22	3d3.(2D2).4s	1D	2	3d3.(2F).4p	3F*	2	220620.8	302292.5	1224.4142	0.0020			1.6e-03	4.31E+09	1613	
23	3d3.(4P).4s	5P	1	3d3.(2D2).4p	3F*	2	204729.7	286154.6	1228.1263	0.0016			5.9e-05 \dagger	5.92E+09	2799	
24	3d3.(4P).4s	3P	2	3d3.(4P).4p	3S*	1	213649.0	294643.9	1234.6455	0.0022	1234.6417	0.0024	9.6e-02	8.47E+09	2338	
25	3d3.(4F).4s	3F	3	3d3.(4P).4p	5D*	2	195933.2	276759.1	1237.2272	0.0017			1.2e-04 \dagger	1.85E+09	2351	
26	3d3.(2P).4s	3P	1	3d3.(4P).4p	3S*	1	214611.3	294643.9	1249.4897	0.0022			9.0e-03	8.47E+09	2922	
27	3d3.(2D1).4s	1D	2	3d3.(2D1).4p	1P*	1	262509.1	342462.1	1250.7350	\star	0.0040		1.8e-01	8.62E+09	2380	
28	3d3.(4F).4s	5F	4	3d3.(4F).4p	3F*	3	187719.0	267240.5	1257.5222	0.0022			3.3e-04 \dagger	5.10E+09	2416	
29	3d3.(4F).4s	5F	3	3d3.(4F).4p	3F*	2	187157.6	266612.9	1258.5696	0.0021			1.9e-05 \dagger	5.10E+09	2300	
30	3d3.(4P).4p	3D*	3	3d3.(4F).4d	3F	2	286431.1	365556.0	1263.8250	0.0060			8.6e-04 \dagger	1.12E+10 \dagger		
31	3d3.(4P).4s	5P	1	3d3.(2D2).4p	3P*	2	204729.7	283686.1	1266.5218	0.0015			1.1e-02	4.67E+09	3653	
32	3d3.(2G).4s	1G	4	3d3.(2H).4p	3G*	5	213533.9	292287.3	1269.7855	0.0016			5.1e-03	8.20E+09	3697	
33	3d3.(4P).4s	5P	2	3d3.(2D2).4p	3P*	2	204975.2	283686.1	1270.4713	0.0015			1.1e-02	4.67E+09	3444	
34	3d3.(2G).4s	3G	4	3d3.(2H).4p	3I*	5	209109.9	287440.4	1276.6419	0.0020			1.4e-03	2.11E+09	2461	
35	3d3.(4P).4s	5P	3	3d3.(2D2).4p	3P*	2	205536.2	283686.1	1279.5917	0.0016			1.0e-02	4.67E+09	2748	
36	3d3.(2G).4s	3G	5	3d3.(2D2).4p	3F*	4	209523.7	287620.2	1280.4678	\star	0.0021	1280.4711	0.0031	2.6e-02	5.65E+09	2373
37	3d3.(4P).4s	3P	1	3d3.(2D2).4p	3P*	0	212818.0	290903.4	1280.6480	0.0030			1.1e-02	8.06E+09	3705	
38	3d3.(4P).4s	3P	0	3d3.(2D2).4p	3P*	1	212542.0	290583.6	1281.3672	\star	0.0022		9.7e-02	7.94E+09	3640	
39	3d3.(2G).4s	3G	3	3d3.(4P).4p	3D*	2	208838.0	286862.5	1281.6471	0.0016	1281.6518	0.0038	6.7e-03	6.41E+09	3128	
40	3d3.(2G).4s	3G	4	3d3.(2P).4p	3F*	3	209109.9	287109.4	1282.0587	0.0018			1.0e-02	6.62E+09	3055	
41	3d3.(2F).4s	3F	4	3d3.(2F).4p	1F*	3	233633.5	311538.4	1283.6150	0.0030			3.4e-03	1.00E+10		
42	3d3.(4P).4s	5P	1	3d3.(2P).4p	1D*	2	204729.7	282604.8	1284.1080	0.0017	1284.1069	0.0024	4.6e-02	2.29E+09	2596	

Table A1 Continued: Summary of laboratory and Ritz wavelength

ID	C1	T1	J1	C2	T2	J2	E1 (cm ⁻¹)	E2 (cm ⁻¹)	K14		W19		f	$\Gamma(\text{ s}^{-1})$	$q(\text{ cm}^{-1})$		
									$\lambda(\text{\AA})$	$\delta\lambda(\text{\AA})$	$\lambda(\text{\AA})$	$\delta\lambda(\text{\AA})$					
43	3d3.(4P).4s	3P	1	3d3.(2D2).4p	3P*	1	212818.0	290583.6	1285.9150	★	0.0021	1285.9205	◇	0.0026	4.2e-02	7.94E+09	3386
44	3d3.(4P).4s	5P	1	3d3.(4P).4p	5S*	2	204729.7	282423.2	1287.1090	0.0016	1287.109	0.0026	4.8e-02	1.35E+09	2681		
45	3d3.(4P).4s	5P	2	3d3.(2P).4p	1D*	2	204975.2	282604.8	1288.1681	★	0.0018	1288.164	◇	0.0024	4.9e-02	2.29E+09	2387
46	3d3.(4P).4s	5P	2	3d3.(2G).4p	1F*	3	204975.2	282571.4	1288.7231	0.0018			1.0e-06 [†]	3.61E+09	3436		
47	3d3.(2F).4s	3F	4	3d3.(2F).4p	1G*	4	233633.5	311180.7	1289.5369	0.0024			1.1e-03	5.00E+09	2798		
48	3d3.(4P).4s	5P	2	3d3.(4P).4p	5S*	2	204975.2	282423.2	1291.1881	★	0.0017	1291.1903	◇	0.0024	4.2e-02	1.35E+09	2472
49	3d3.(2F).4s	3F	3	3d3.(2F).4p	1G*	4	233848.7	311180.7	1293.1270	0.0020			3.1e-03	5.00E+09	2635		
50	3d3.(2G).4s	3G	4	3d3.(4P).4p	3D*	3	209109.9	286431.1	1293.3059	★	0.0017	1293.2933	0.01	1.6e-02	5.62E+09	2665	
51	3d3.(2G).4s	3G	3	3d3.(2D2).4p	3F*	2	208838.0	286154.6	1293.3826	★	0.0018	1293.3776	0.0024	3.4e-02	5.92E+09	2588	
52	3d3.(4P).4s	5P	3	3d3.(2P).4p	1D*	2	205536.2	282604.8	1297.5453	★	0.0018	1297.5439	◇	0.0024	3.9e-02	2.29E+09	1691
53	3d3.(4P).4s	5P	3	3d3.(4P).4p	5S*	2	205536.2	282423.2	1300.6095	★	0.0017	1300.6052	0.0024	4.2e-02	1.35E+09	1776	
54	3d3.(2D1).4s	3D	1	3d3.(2D1).4p	3P*	0	258769.6	335642.7	1300.8450	0.0040	1300.8432	0.0024	9.8e-02	4.15E+09	3149		
55	3d3.(4F).4s	5F	3	3d3.(4F).4p	3G*	3	187157.6	263898.7	1303.0834	0.0021			2.2e-03	5.05E+09	2290		
56	3d3.(4F).4s	5F	5	3d3.(4F).4p	3G*	5	188395.4	265112.8	1303.4853	0.0024	1303.4815	0.0031	1.6e-02	4.98E+09	2375		
57	3d3.(2D1).4s	3D	2	3d3.(2D1).4p	3P*	1	258628.6	335267.9	1304.8140	0.0030	1304.8315	0.0055	1.2e-01	4.17E+09	2979		
58	3d3.(4P).4s	3P	1	3d3.(2D2).4p	3D*	2	212818.0	289389.5	1305.9674	0.0018	1305.9341	0.01	3.4e-02	6.02E+09	3143		
59	3d3.(2G).4s	1G	4	3d3.(2H).4p	1H*	5	213533.9	290098.8	1306.0803	0.0020	1306.0792	0.0024	6.9e-02	1.17E+10	2541		
60	3d3.(2D1).4s	3D	1	3d3.(2D1).4p	3P*	1	258769.6	335267.9	1307.2190	0.0030	1307.2216	0.0024	9.6e-02	4.17E+09	2862		
61	3d3.(2P).4s	1P	1	3d3.(2P).4p	1P*	1	219486.7	295973.0	1307.4242	★	0.0023	1307.4237	◇	0.0024	2.2e-01	6.80E+09	2311
62	3d3.(2G).4s	3G	4	3d3.(2P).4p	3D*	3	209109.9	285474.0	1309.5147	0.0020			1.1e-02	5.65E+09	2992		
63	3d3.(2P).4s	3P	1	3d3.(2D2).4p	3P*	0	214611.3	290903.4	1310.7510	0.0030			6.0e-04	8.06E+09	3286		
64	3d3.(4P).4s	3P	2	3d3.(2D2).4p	3D*	3	213649.0	289912.8	1311.2378	0.0019	1311.2293	0.0074	3.8e-02	5.88E+09	2389		
65	3d3.(2P).4s	1P	1	3d3.(2D2).4p	1D*	2	219486.7	295716.2	1311.8290	★	0.0030	1311.8278	◇	0.0024	1.9e-01	1.01E+10	1616
66	3d3.(4P).4s	3P	0	3d3.(2D2).4p	3D*	1	212542.0	288669.5	1313.5851	★	0.0023		6.6e-02	6.17E+09	2507		
67	3d3.(2G).4s	3G	3	3d3.(2P).4p	3D*	2	208838.0	284911.0	1314.5256	★	0.0017	1314.5292	◇	0.0026	2.2e-03	5.21E+09	2920
68	3d3.(2D1).4s	3D	2	3d3.(2D1).4p	3P*	2	258628.6	334509.2	1317.8610	0.0030	1317.8611	0.0024	7.0e-02	4.20E+09			
69	3d3.(2G).4s	3G	3	3d3.(2H).4p	3H*	4	208838.0	284690.3	1318.3505	0.0021	1318.3488	0.0024	6.0e-02	5.99E+09	3660		
70	3d3.(4P).4s	3P	1	3d3.(2D2).4p	3D*	1	212818.0	288669.5	1318.3648	0.0023			5.8e-02	6.17E+09	2253		
71	3d3.(2D1).4s	3D	1	3d3.(2D1).4p	3P*	2	258769.6	334509.2	1320.3150	0.0030			1.2e-02	4.20E+09			
72	3d3.(2H).4s	3H	4	3d3.(2H).4p	3G*	3	216779.1	292513.1	1320.4116	0.0020	1320.4119	0.0024	1.9e-01	8.00E+09	2419		
73	3d3.(2G).4s	3G	4	3d3.(2H).4p	3H*	5	209109.9	284790.5	1321.3424	0.0020	1321.3381	0.0024	7.2e-02	5.78E+09	2588		
74	3d3.(2G).4s	3G	5	3d3.(2H).4p	3H*	6	209523.7	285195.8	1321.4905	0.0023	1321.4887	0.0024	8.5e-02	5.81E+09	2559		
75	3d3.(2H).4s	3H	4	3d3.(2H).4p	3G*	4	216779.1	292430.6	1321.8507	★	0.0022	1321.8476	◇	0.0024	2.1e-02	7.75E+09	2296
76	3d3.(2G).4s	3G	4	3d3.(2H).4p	3H*	4	209109.9	284690.3	1323.0938	0.0019			1.1e-03	5.99E+09	3435		
77	3d3.(2H).4s	3H	5	3d3.(2H).4p	3G*	4	216860.2	292430.6	1323.2693	0.0020	1323.2685	0.0024	1.8e-01	7.75E+09	2831		
78	3d3.(2H).4s	3H	5	3d3.(2H).4p	1I*	6	216860.2	292365.6	1324.4086	0.0021			6.3e-03	4.98E+09	2626		
79	3d3.(2H).4s	3H	5	3d3.(2H).4p	3G*	5	216860.2	292287.3	1325.7838	★	0.0017	1325.781	◇	0.0031	2.0e-02	8.20E+09	2978
80	3d3.(2D2).4s	1D	2	3d3.(2P).4p	1P*	1	220620.8	295973.0	1327.1006	0.0023	1327.1012	0.0024	3.2e-02	6.80E+09	3006		
81	3d3.(2H).4s	3H	6	3d3.(2H).4p	1I*	6	217122.3	292365.6	1329.0215	0.0021			3.3e-03	4.98E+09	2410		
82	3d3.(2H).4s	3H	6	3d3.(2H).4p	3G*	5	217122.3	292287.3	1330.4063	0.0018	1330.4025	0.0024	1.9e-01	8.20E+09	2762		
83	3d3.(2D2).4s	3D	1	3d3.(2D2).4p	3P*	0	215782.4	290903.4	1331.1860	★	0.0030	1331.1765	0.0031	7.6e-02	8.06E+09	3763	
84	3d3.(2D2).4s	1D	2	3d3.(2D2).4p	1D*	2	220620.8	295716.2	1331.6390	★	0.0030	1331.6376	◇	0.0024	1.6e-01	1.01E+10	2311
85	3d3.(4P).4s	3P	2	3d3.(2D2).4p	3D*	1	213649.0	288669.5	1332.9697	0.0022			1.3e-03	6.17E+09	1250		
86	3d3.(2G).4s	3G	3	3d3.(2D2).4p	3P*	2	208838.0	283686.1	1336.0377	0.0016			2.5e-03	4.67E+09	3442		
87	3d3.(2P).4s	3P	1	3d3.(2D2).4p	3D*	2	214611.3	289389.5	1337.2869	0.0019	1337.2865	0.0024	3.5e-02	6.02E+09	2724		
88	3d3.(2D2).4s	3D	3	3d3.(2D2).4p	1F*	3	216538.0	291231.3	1338.8076	★	0.0022	1338.7994	0.0038	2.9e-02	9.26E+09	2389	
89	3d3.(2F).4s	3F	2	3d3.(2F).4p	3D*	1	234027.1	308671.3	1339.6900	★	0.0030	1339.6779	0.0038	1.6e-01	6.37E+09	3128	
90	3d3.(4F).4s	5F	2	3d3.(4F).4p	3D*	3	186725.7	261179.7	1343.1108	0.0022			6.3e-03	3.62E+09	3492		
91	3d3.(2F).4s	3F	3	3d3.(2F).4p	3D*	2	233848.7	308164.8	1345.6040	0.0030	1345.6036	0.0031	1.5e-01	5.99E+09			
92	3d3.(2F).4s	3F	2	3d3.(2F).4p	3D*	2	234027.1	308164.8	1348.8420	0.0030	1348.8203	0.01	4.0e-02	5.99E+09			
93	3d3.(4P).4s	3P	1	3d3.(4P).4p	3D*	2	212818.0	286862.5	1350.5374	★	0.0016	1350.525	0.0031	1.3e-01	6.41E+09	3306	
94	3d3.(4P).4s	3P	1	3d3.(4P).4p	3D*	1	212818.0	286855.2	1350.6724	0.0017			1.7e-02	6.49E+09	3254		
95	3d3.(4F).4s	5F	3	3d3.(4F).4p	3D*	3	187157.6	261179.7	1350.9483	0.0020			2.5e-03	3.62E+09	2998		
96	3d3.(4F).4s	5F	1	3d3.(4F).4p	3D*	2	186433.8	260411.6	1351.7563	0.0024	1351.7366	0.0038	2.8e-02	3.64E+09	3437		
97	3d3.(2F).4s	1F	3	3d3.(2F).4p	1F*	3	237729.3	311538.4	1354.8450	0.0030	1354.8432	0.0026	2.6e-01	1.00E+10			
98	3d3.(2G).4s	3G	3	3d3.(2P).4p	1D*	2	208838.0	282604.8	1355.6223	0.0019	1355.6233	0.0024	1.8e-02	2.29E+09	2385		
99	3d3.(2G).4s	3G	3	3d3.(2G).4p	1F*	3	208838.0	282571.4	1356.2369	0.0018			2.6e-03	3.61E+09	3434		
100	3d3.(4F).4s	5F	2	3d3.(4F).4p	3D*	2	186725.7	260411.6	1357.1121	0.0023			2.0e-02	3.64E+09	3107		
101	3d3.(2F).4s	3F	4	3d3.(2F).4p	3D*	3	233848.7	307288.7	1357.6760	0.0030	1357.672	0.0024	1.6e-01	6.21E+09			

Table A1 Continued: Summary of laboratory and Ritz wavelength

ID	C1	T1	J1	C2	T2	J2	E1 (cm^{-1})	E2 (cm^{-1})	K14		W19		f	$\Gamma(\text{s}^{-1})$	$q(\text{cm}^{-1})$
									$\lambda(\text{\AA})$	$\delta\lambda(\text{\AA})$	$\lambda(\text{\AA})$	$\delta\lambda(\text{\AA})$			
110	3d3.(2D1).4s	1D	2	3d3.(2D1).4p	1F*	3	262509.1	335947.2	1361.6910	0.0040	1361.6866	0.0026	3.8e-01	6.14E+09	
111	3d3.(2F).4s	3F	4	3d3.(2F).4p	3G*	5	233633.5	307064.1	1361.8280	★ 0.0040	1361.8239	◇ 0.0024	3.2e-01	3.05E+09	3100
112	3d3.(2D2).4s	3D	3	3d3.(2D2).4p	3D*	3	216538.0	289912.8	1362.8639	0.0021	1362.8615	0.0024	1.4e-01	5.88E+09	2361
113	3d3.(4F).4s	5F	3	3d3.(4F).4p	5F*	4	187157.6	260521.1	1363.0758	0.0023	1363.076	0.0024	9.2e-02	3.85E+09	3504
114	3d3.(2G).4s	3G	5	3d3.(2G).4p	1H*	5	209523.7	282871.6	1363.3665	0.0019			9.4e-03	2.37E+09	2090
115	3d3.(4F).4s	5F	4	3d3.(4F).4p	5F*	5	187719.0	261052.0	1363.6431	0.0023	1363.6416	0.0024	5.8e-02	3.37E+09	3206
116	3d3.(4F).4s	5F	2	3d3.(4F).4p	5F*	1	186725.7	259995.4	1364.8201	★ 0.0023	1364.8055	0.0038	4.4e-02	3.64E+09	2960
117	3d3.(2F).4s	3F	2	3d3.(2F).4p	3D*	3	234027.1	307288.7	1364.9720	0.0040	1364.9787	0.0026	1.5e-02	6.21E+09	1860
118	3d3.(2D2).4s	3D	2	3d3.(2D2).4p	3D*	3	216652.0	289912.8	1364.9850	0.0030			1.1e-01	5.88E+09	
119	3d3.(4F).4s	5F	3	3d3.(4F).4p	3D*	2	187157.6	260411.6	1365.1143	0.0023	1365.1168	0.0024	4.7e-02	3.64E+09	2613
120	3d3.(4F).4s	5F	2	3d3.(4F).4p	5F*	3	186725.7	259955.0	1365.5742	0.0024	1365.5685	0.0038	1.1e-01	4.95E+09	4562
121	3d3.(4P).4s	3P	2	3d3.(4P).4p	3D*	2	213649.0	286862.5	1365.8679	0.0016			2.7e-02	6.41E+09	2303
122	3d3.(4P).4s	3P	1	3d3.(2D2).4p	1P*	1	212818.0	285961.4	1367.1757	0.0020			1.6e-02	6.90E+09	3037
123	3d3.(2H).4s	3H	6	3d3.(2H).4p	1H*	5	217122.3	290098.8	1370.3038	★ 0.0022	1370.2998	◇ 0.0024	1.4e-02	1.17E+10	1606
124	3d3.(4F).4s	5F	1	3d3.(4F).4p	5F*	2	186433.8	259376.3	1370.9419	★ 0.0022	1370.9449	◇ 0.0024	8.9e-02	6.02E+09	3905
125	3d3.(2G).4s	3G	4	3d3.(2G).4p	1G*	4	209109.9	282037.7	1371.2188	0.0022			1.3e-02	5.95E+09	2272
126	3d3.(2D2).4s	3D	1	3d3.(2D2).4p	3D*	1	215782.4	288669.5	1371.9858	★ 0.0023	1371.9871	◇ 0.0024	1.4e-01	6.17E+09	2311
127	3d3.(2D2).4s	3D	3	3d3.(2D2).4p	3D*	2	216538.0	289389.5	1372.6536	0.0020			1.4e-02	6.02E+09	2112
128	3d3.(4F).4s	5F	4	3d3.(4F).4p	5F*	4	187719.0	260521.1	1373.5868	★ 0.0023	1373.591	0.0024	2.0e-01	3.85E+09	2869
129	3d3.(4F).4s	5F	3	3d3.(4F).4p	5F*	3	187157.6	259955.0	1373.6770	★ 0.0020	1373.6799	0.0038	2.0e-01	4.95E+09	4068
130	3d3.(4P).4s	3P	2	3d3.(4P).4p	3D*	3	213649.0	286431.1	1373.9646	★ 0.0018	1373.9654	◇ 0.0024	1.5e-01	5.62E+09	2065
131	3d3.(2F).4s	3F	3	3d3.(2F).4p	3G*	4	233848.7	306622.7	1374.1180	★ 0.0030	1374.1175	◇ 0.0024	3.3e-01	2.99E+09	2569
132	3d3.(2H).4s	3H	4	3d3.(2H).4p	1G*	4	216779.1	289546.0	1374.2518	0.0024			5.5e-03	3.56E+09	2565
133	3d3.(2D1).4s	3D	2	3d3.(2D1).4p	3F*	3	258628.6	331367.3	1374.7850	0.0060	1374.786	0.0024	3.7e-01	3.65E+09	
134	3d3.(2D2).4s	3D	2	3d3.(2D2).4p	3D*	2	216652.0	289389.5	1374.8050	0.0040			1.2e-01	6.02E+09	
135	3d3.(2H).4s	3H	5	3d3.(2H).4p	1G*	4	216860.2	289546.0	1375.7851	0.0023	1375.7876	0.0024	9.7e-03	3.56E+09	3100
136	3d3.(4F).4s	5F	5	3d3.(4F).4p	5F*	5	188395.4	261052.0	1376.3367	0.0024	1376.3384	0.0024	2.2e-01	3.37E+09	2442
137	3d3.(4F).4s	5F	2	3d3.(4F).4p	5F*	2	186725.7	259376.3	1376.4511	0.0020	1376.4499	0.0038	1.9e-01	6.02E+09	3575
138	3d3.(2P).4s	3P	2	3d3.(2P).4p	3F*	3	214525.6	287109.4	1377.7171	0.0020			1.3e-02	6.62E+09	3159
139	3d3.(2D1).4s	3D	1	3d3.(2D1).4p	3F*	2	258769.6	331333.8	1378.0920	0.0040	1378.092	0.0024	3.5e-01	4.41E+09	
140	3d3.(4P).4s	5P	3	3d3.(4P).4p	5D*	4	205536.2	278075.6	1378.5620	★ 0.0030	1378.5584	◇ 0.0024	3.5e-01	1.33E+09	3217
141	3d3.(4P).4s	3P	2	3d3.(2D2).4p	3F*	2	213649.0	286154.6	1379.2046	0.0019			9.6e-03	5.92E+09	1763
142	3d3.(4F).4s	5F	1	3d3.(4F).4p	5D*	1	186433.8	258891.5	1380.1140	★ 0.0030	1380.1107	◇ 0.0024	1.9e-01	7.25E+09	3200
143	3d3.(2F).4s	3F	3	3d3.(2F).4p	3G*	3	233848.7	306193.8	1382.2640	0.0040			7.5e-03	2.95E+09	2112
144	3d3.(2P).4s	3P	2	3d3.(4P).4p	3D*	2	214525.6	286862.5	1382.4192	0.0017			1.6e-02	6.41E+09	3007
145	3d3.(2P).4s	3P	2	3d3.(4P).4p	3D*	1	214525.6	286855.2	1382.5606	0.0018			5.6e-03	6.49E+09	2955
146	3d3.(2P).4s	3P	1	3d3.(4P).4p	3D*	2	214611.3	286862.5	1384.0585	0.0017	1384.0453	0.0055	5.6e-02	6.41E+09	2887
147	3d3.(2P).4s	3P	1	3d3.(4P).4p	3D*	1	214611.3	286855.2	1384.2003	0.0018	1384.2075	0.0038	4.8e-02	6.49E+09	2835
148	3d3.(4F).4s	5F	3	3d3.(4F).4p	5F*	2	187157.6	259376.3	1384.6837	0.0019	1384.6974	0.01	8.9e-03	6.02E+09	3081
149	3d3.(4F).4s	5F	1	3d3.(4F).4p	5D*	0	186433.8	258619.7	1385.3120	★ 0.0040	1385.3136	◇ 0.0024	8.9e-02	8.40E+09	3108
150	3d3.(2F).4s	3F	2	3d3.(2F).4p	3G*	3	234027.1	306193.8	1385.6810	0.0040	1385.6833	0.0024	3.4e-01	2.95E+09	1965
151	3d3.(4F).4s	5F	2	3d3.(4F).4p	5D*	1	186725.7	258891.5	1385.6980	0.0030			4.0e-02	7.25E+09	2870
152	3d3.(4F).4s	5F	5	3d3.(4F).4p	5F*	4	188395.4	260521.1	1386.4670	0.0024			1.6e-03	3.85E+09	2105
153	3d3.(4P).4s	5P	2	3d3.(4P).4p	5D*	3	204975.2	277068.4	1387.0940	0.0030	1387.0913	0.0024	2.9e-01	1.54E+09	2911
154	3d3.(4P).4s	3P	1	3d3.(2P).4p	3D*	2	212818.0	284911.0	1387.0959	0.0018			7.7e-02	5.21E+09	3098
155	3d3.(2H).4s	3H	6	3d3.(2H).4p	3I*	7	217122.3	289171.6	1387.9380	0.0030	1387.9376	0.0024	3.2e-01	1.58E+09	
156	3d3.(4F).4s	3F	2	3d3.(4F).4p	3F*	3	195196.5	267240.5	1388.0401	★ 0.0024			1.5e-02	5.10E+09	3359
157	3d3.(4P).4s	5P	1	3d3.(4P).4p	3P*	1	204729.7	276765.8	1388.1938	★ 0.0018	1388.1934	◇ 0.0024	1.1e-01	2.12E+09	3543
158	3d3.(4P).4s	5P	1	3d3.(4P).4p	5D*	2	204729.7	276759.1	1388.3235	★ 0.0018	1388.3268	◇ 0.0024	1.9e-01	1.85E+09	3033
159	3d3.(2G).4s	3G	3	3d3.(2G).4p	3F*	3	208838.0	280831.9	1389.0048	0.0019			8.1e-02	6.25E+09	2922
160	3d3.(4F).4s	5F	2	3d3.(4F).4p	5D*	3	186725.7	258680.1	1389.7693	0.0021			2.3e-03	6.76E+09	2666
161	3d3.(2P).4s	3P	2	3d3.(4P).4p	3D*	3	214525.6	286431.1	1390.7138	0.0018	1390.7206	0.0038	2.1e-02	5.62E+09	2769
162	3d3.(2D2).4s	1D	2	3d3.(2H).4p	3G*	3	220620.8	292513.1	1390.9690	0.0020			2.3e-02	8.00E+09	2657
163	3d3.(4P).4s	3P	2	3d3.(2P).4p	3D*	3	213649.0	285474.0	1392.2725	0.0023			2.4e-02	5.65E+09	2392
164	3d3.(4P).4s	5P	2	3d3.(4P).4p	3P*	1	204975.2	276765.8	1392.9400	0.0019			7.9e-03	2.12E+09	3334
165	3d3.(4P).4s	5P	2	3d3.(4P).4p	5D*	2	204975.2	276759.1	1393.0706	★ 0.0019	1393.0739	◇ 0.0031	7.4e-02	1.85E+09	2824
166	3d3.(2G).4s	3G	4	3d3.(2G).4p	3F*	3	209109.9	280831.9	1394.2712	★ 0.0019	1394.265	0.0038	1.0e-01	6.25E+09	2697
167	3d3.(4P).4s	5P	1	3d3.(4P).4p	5D*	0	204729.7	276434.8	1394.6013	0.0022			4.6e-02	2.18E+09	2555
168	3d3.(2G).4s	3G	3	3d3.(2G).4p	3F*	2	208838.0	280539.6	1394.6686	0.0019	1394.6674	0.0024	1.2e-01	5.92E+09	3206
169	3d3.(2P).4s	3P	2	3d3.(2P).4p	3S*	1	214525.6	286187.5	1395.4411	0.0019					

Table A1 Continued: Summary of laboratory and Ritz wavelength

ID	C1	T1	J1	C2	T2	J2	E1 (cm ⁻¹)	E2 (cm ⁻¹)	K14		W19		f	$\Gamma(\text{ s}^{-1})$	$q(\text{ cm}^{-1})$
									$\lambda(\text{\AA})$	$\delta\lambda(\text{\AA})$	$\lambda(\text{\AA})$	$\delta\lambda(\text{\AA})$			
177	3d3.(2H).4s	3H	5	3d3.(2H).4p	3I*	6	216860.2	288167.0	1402.3910	0.0030	1402.3946	0.0038	3.2e-01	1.80E+09	2425
178	3d3.(2G).4s	3G	4	3d3.(2G).4p	3F*	4	209109.9	280366.9	1403.3697	0.0020	1403.368	0.0024	5.8e-02	6.67E+09	2021
179	3d3.(2G).4s	1G	4	3d3.(2H).4p	3H*	5	213533.9	284790.5	1403.3780	0.0024			4.0e-06 [†]	5.78E+09	2983
180	3d3.(4P).4s	5P	3	3d3.(4P).4p	5D*	2	205536.2	276759.1	1404.0438	0.0019			4.1e-03	1.85E+09	2128
181	3d3.(4P).4s	3P	0	3d3.(2P).4p	3D*	1	212542.0	283753.9	1404.2589	★ 0.0020	1404.2665	◇ 0.0038	1.8e-01	5.29E+09	1970
182	3d3.(4F).4s	3F	4	3d3.(4F).4p	3F*	4	196838.7	267928.5	1406.6710	0.0030	1406.6695	0.0024	2.5e-01	5.10E+09	2222
183	3d3.(2D2).4s	3D	3	3d3.(2D2).4p	3F*	4	216538.0	287620.2	1406.8220	0.0030	1406.8232	0.0024	3.0e-01	5.65E+09	2157
184	3d3.(2D2).4s	3D	1	3d3.(4P).4p	3D*	1	215782.4	286855.2	1407.0098	0.0019			3.8e-02	6.49E+09	3312
185	3d3.(2H).4s	1H	5	3d3.(2H).4p	1I*	6	221304.9	292365.6	1407.2470	★ 0.0030	1407.2451	◇ 0.0024	3.2e-01	4.98E+09	2471
186	3d3.(2H).4s	3H	6	3d3.(2H).4p	3I*	6	217122.3	288167.0	1407.5640	0.0030			2.0e-03	1.80E+09	2209
187	3d3.(4F).4s	5F	2	3d3.(4F).4p	3D*	1	186725.7	257742.4	1408.1190	★ 0.0030	1408.1202	◇ 0.0024	7.8e-02	4.72E+09	1343
188	3d3.(2H).4s	1H	5	3d3.(2H).4p	3G*	5	221304.9	292287.3	1408.7993	★ 0.0022			1.7e-02	8.20E+09	2823
189	3d3.(4F).4s	5F	3	3d3.(4F).4p	5D*	2	187157.6	258128.7	1409.0254	0.0021	1409.0288	0.0024	1.3e-01	5.85E+09	1409
190	3d3.(4F).4s	5F	4	3d3.(4F).4p	5D*	3	187719.0	258680.1	1409.2236	★ 0.0021	1409.223	0.0024	1.8e-01	6.76E+09	1537
191	3d3.(4F).4s	5F	5	3d3.(4F).4p	5D*	4	188395.4	259345.0	1409.4510	0.0030	1409.4539	0.0024	2.1e-01	7.52E+09	1628
192	3d3.(4P).4s	3P	1	3d3.(2P).4p	3D*	1	212818.0	283753.9	1409.7226	0.0018			3.1e-02	5.29E+09	1716
193	3d3.(2G).4s	3G	4	3d3.(2G).4p	3G*	5	209109.9	280039.5	1409.8484	★ 0.0019	1409.8407	0.0038	6.3e-02	7.58E+09	2845
194	3d3.(4P).4s	3P	1	3d3.(2D2).4p	3P*	2	212818.0	283686.1	1411.0703	0.0016	1411.059	0.0047	1.6e-02	4.67E+09	3620
195	3d3.(2G).4s	3G	5	3d3.(2G).4p	3F*	4	209523.7	280366.9	1411.5675	★ 0.0021	1411.5659	◇ 0.0024	7.4e-02	6.67E+09	1609
196	3d3.(4F).4s	3F	3	3d3.(4F).4p	3F*	2	195933.2	266612.9	1414.8320	★ 0.0030	1414.8424	0.0074	3.0e-02	5.10E+09	1764
197	3d3.(2G).4s	3G	3	3d3.(2G).4p	3G*	4	208838.0	279502.4	1415.1381	0.0019			4.6e-02	7.46E+09	2593
198	3d3.(2H).4s	3H	4	3d3.(2H).4p	3I*	5	216779.1	287440.4	1415.2028	0.0024	1415.1918	0.01	3.3e-01	2.11E+09	1602
199	3d3.(2D2).4s	1D	2	3d3.(2D2).4p	1F*	3	220620.8	291231.3	1416.2196	★ 0.0024	1416.2244	◇ 0.0024	2.6e-01	9.26E+09	2396
200	3d3.(2H).4s	3H	5	3d3.(2H).4p	3I*	5	216860.2	287440.4	1416.8290	0.0023			1.4e-03	2.11E+09	2137
201	3d3.(2D2).4s	3D	3	3d3.(2P).4p	3F*	3	216538.0	287109.4	1417.0030	0.0021			1.4e-02	6.62E+09	2427
202	3d3.(2G).4s	3G	5	3d3.(2G).4p	3G*	5	209523.7	280039.5	1418.1223	0.0020	1418.1281	0.0038	1.8e-01	7.58E+09	2433
203	3d3.(2D2).4s	3D	2	3d3.(2P).4p	3F*	3	216652.0	287109.4	1419.2960	0.0040			1.9e-01	6.62E+09	
204	3d3.(4P).4s	5P	1	3d3.(4P).4p	5D*	1	204729.7	275146.5	1420.1161	0.0019	1420.1262	0.0038	9.8e-02	2.09E+09	1581
205	3d3.(4F).4s	3F	4	3d3.(4F).4p	3F*	3	196838.7	267240.5	1420.4180	★ 0.0030			2.7e-02	5.10E+09	1509
206	3d3.(4P).4s	5P	2	3d3.(4P).4p	3P*	2	204975.2	275374.1	1420.4765	★ 0.0020	1420.4576	0.0055	8.1e-02	2.60E+09	1758
207	3d3.(2G).4s	3G	4	3d3.(2G).4p	3G*	4	209109.9	279502.4	1420.6049	★ 0.0018	1420.6058	◇ 0.0026	1.3e-01	7.46E+09	2368
208	3d3.(2P).4s	3P	2	3d3.(2P).4p	3D*	2	214525.6	284911.0	1420.7486	0.0018	1420.7587	0.01	2.7e-02	5.21E+09	2799
209	3d3.(2D2).4s	3D	1	3d3.(2D2).4p	3F*	2	215782.4	286154.6	1421.0167	★ 0.0020	1421.0309	0.0074	9.4e-02	5.92E+09	2824
210	3d3.(2D2).4s	3D	3	3d3.(4P).4p	3D*	2	216538.0	286862.5	1421.9775	0.0018			2.4e-03	6.41E+09	2275
211	3d3.(2P).4s	3P	1	3d3.(2P).4p	3D*	2	214611.3	284911.0	1422.4802	★ 0.0018	1422.483	◇ 0.0024	1.6e-01	5.21E+09	2679
212	3d3.(2D2).4s	3D	2	3d3.(4P).4p	3D*	2	216652.0	286862.5	1424.2870	0.0030			3.3e-04 [†]	6.41E+09	
213	3d3.(4P).4s	5P	2	3d3.(4P).4p	5D*	1	204975.2	275146.5	1425.0834	★ 0.0020	1425.0886	◇ 0.0031	2.9e-02	2.09E+09	1372
214	3d3.(4P).4s	3P	2	3d3.(2P).4p	3D*	1	213649.0	283753.9	1426.4346	0.0018			1.0e-03	5.29E+09	713
215	3d3.(4P).4s	3P	2	3d3.(2D2).4p	3P*	2	213649.0	283686.1	1427.8145	0.0016	1427.8252	0.0038	2.6e-02	4.67E+09	2617
216	3d3.(4P).4s	5P	1	3d3.(4P).4p	3P*	0	204729.7	274753.0	1428.0960	0.0030	1428.0981	0.0026	4.1e-02	1.89E+09	1245
217	3d3.(2G).4s	3G	5	3d3.(2G).4p	3G*	4	209523.7	279502.4	1429.0058	0.0020	1429.0059	0.0024	5.5e-02	7.46E+09	1956
218	3d3.(2D2).4s	1D	2	3d3.(2D2).4p	3P*	1	220620.8	290583.6	1429.3300	0.0030			4.8e-03	7.94E+09	2362
219	3d3.(2G).4s	3G	3	3d3.(2G).4p	3G*	3	208838.0	278794.0	1429.4691	0.0021			1.6e-01	7.63E+09	1730
220	3d3.(2F).4s	1F	3	3d3.(2F).4p	1D*	2	237729.3	307644.0	1430.3130	★ 0.0030	1430.3215	0.0055	1.4e-01	4.78E+09	2449
221	3d3.(4F).4s	5F	5	3d3.(4F).4p	5G*	6	188395.4	258297.4	1430.5730	0.0030	1430.5672	0.0031	3.2e-01	8.70E+08	3207
222	3d3.(2D2).4s	3D	3	3d3.(4P).4p	3D*	3	216538.0	286431.1	1430.7552	★ 0.0019	1430.7793	0.0074	7.7e-02	5.62E+09	2037
223	3d3.(4P).4s	5P	3	3d3.(4P).4p	3P*	2	205536.2	275374.1	1431.8875	0.0019			7.2e-03	2.60E+09	1062
224	3d3.(4P).4s	3P	1	3d3.(2P).4p	1D*	2	212818.0	282604.8	1432.9345	0.0020			2.1e-02	2.29E+09	2563
225	3d3.(2D2).4s	1D	2	3d3.(2P).4p	3P*	2	220620.8	290406.9	1432.9490	0.0050			1.0e-03	7.63E+09	2035
226	3d3.(2G).4s	3G	4	3d3.(2G).4p	3G*	3	209109.9	278794.0	1435.0474	★ 0.0020	1435.0334	0.0074	5.0e-02	7.63E+09	1505
227	3d3.(2D2).4s	3D	2	3d3.(2D2).4p	3F*	2	216652.0	286154.6	1438.7950	0.0040			7.2e-02	5.92E+09	
228	3d3.(2D1).4s	3D	3	3d3.(2D1).4p	3D*	3	258434.4	327924.6	1439.0520	0.0040	1439.0558	0.0024	2.4e-01	6.45E+09	
229	3d3.(4F).4s	5F	4	3d3.(4F).4p	5G*	5	187719.0	257138.0	1440.5290	★ 0.0030	1440.5297	◇ 0.0024	2.7e-01	9.52E+08	2780
230	3d3.(4P).4s	5P	1	3d3.(4P).4p	5P*	2	204729.7	274135.9	1440.7939	★ 0.0019	1440.7886	◇ 0.0024	1.6e-01	6.76E+09	2674
231	3d3.(4P).4s	5P	3	3d3.(4P).4p	5P*	3	205536.2	274929.8	1441.0550	0.0030	1441.0491	0.0026	2.0e-01	6.90E+09	2530
232	3d3.(2G).4s	1G	4	3d3.(2G).4p	1H*	5	213533.9	282871.6	1442.2167	0.0021	1442.2274	0.0084	2.5e-01	2.37E+09	2897
233	3d3.(2D2).4s	1D	2	3d3.(2D2).4p	3D*	3	220620.8	289912.8	1443.1662	0.0022	1443.1616	0.0031	2.5e-02	5.88E+09	2368
234	3d3.(2D1).4s	3D	3	3d3.(2D1).4p	3D*	2	258434.4	327605.7	1445.6860	0.0040	1445.6859	0.0024	4.8e-02	6.41E+09	
235	3d3.(4P).4s	5P	2	3d3.(4P).4p	5P*	2	204975.2	274135.9	1445.9072	0.0021			1.9e-02	6.76E+09	2465
236	3d3.(2P).4s	3P	2	3d3.(2D2).4p	3P*	2									

Table A1 Continued: Summary of laboratory and Ritz wavelength

ID	C1	T1	J1	C2	T2	J2	E1 (cm^{-1})	E2 (cm^{-1})	K14		W19		f	$\Gamma (\text{s}^{-1})$	$q (\text{cm}^{-1})$		
									$\lambda (\text{\AA})$	$\delta\lambda (\text{\AA})$	$\lambda (\text{\AA})$	$\delta\lambda (\text{\AA})$					
244	3d3.(2F).4s	3F	4	3d3.(2F).4p	3F*	4	233633.5	302602.3	1449.9290	★	0.0030	1449.9242	◊	0.0024	2.5e-01	4.27E+09	2535
245	3d3.(4P).4s	5P	1	3d3.(4P).4p	5P*	1	204729.7	273642.9	1451.1020	★	0.0030	1451.1056	◊	0.0024	5.8e-02	7.04E+09	2103
246	3d3.(2D1).4s	3D	2	3d3.(2D1).4p	3D*	1	258628.6	327534.0	1451.2660		0.0030				4.9e-02	6.45E+09	1997
247	3d3.(2P).4s	3P	0	3d3.(2P).4p	3D*	1	214895.3	283753.9	1452.2520		0.0040				2.6e-01	5.29E+09	
248	3d3.(2D1).4s	1D	2	3d3.(2D1).4p	3F*	3	262509.1	331367.3	1452.2600		0.0080				7.2e-03	3.65E+09	
249	3d3.(2D1).4s	1D	2	3d3.(2D1).4p	3F*	2	262509.1	331333.8	1452.9680		0.0040				3.8e-02	4.41E+09	
250	3d3.(2H).4s	1H	5	3d3.(2H).4p	1H*	5	221304.9	290098.8	1453.6160	★	0.0030	1453.6212	◊	0.0026	1.9e-01	1.17E+10	1667
251	3d3.(2D1).4s	3D	1	3d3.(2D1).4p	3D*	1	258769.6	327534.0	1454.2410		0.0030	1454.2388		0.0024	1.7e-01	6.45E+09	1880
252	3d3.(2F).4s	3F	3	3d3.(2F).4p	3F*	4	233848.7	302602.3	1454.4700		0.0030				1.5e-03	4.27E+09	2372
253	3d3.(4F).4s	5F	5	3d3.(4F).4p	5G*	5	188395.4	257138.0	1454.7020	★	0.0030	1454.7043	◊	0.0024	4.2e-02	9.52E+08	2016
254	3d3.(4F).4s	3F	2	3d3.(4F).4p	3G*	3	195196.5	263898.7	1455.5570	★	0.0030	1455.5629	◊	0.0047	3.3e-01	5.05E+09	2598
255	3d3.(2H).4s	3H	4	3d3.(2P).4p	3D*	3	216779.1	285474.0	1455.7120		0.0030				4.3e-05 [†]	5.65E+09	2133
256	3d3.(4F).4s	5F	2	3d3.(4F).4p	5G*	3	186725.7	255399.4	1456.1622	★	0.0024	1456.1641	◊	0.0024	2.6e-01	9.26E+08	2067
257	3d3.(4P).4s	5P	2	3d3.(4P).4p	5P*	1	204975.2	273642.9	1456.2890	★	0.0030	1456.2826	◊	0.0038	1.2e-01	7.04E+09	1894
258	3d3.(4P).4s	5P	3	3d3.(4P).4p	5P*	2	205536.2	274135.9	1457.7321		0.0021	1457.7299		0.0024	9.7e-02	6.76E+09	1769
259	3d3.(2F).4s	3F	3	3d3.(2F).4p	3F*	3	233848.7	302376.8	1459.2560	★	0.0030	1459.2552	◊	0.0024	2.1e-01	4.29E+09	2088
260	3d3.(2G).4s	1G	4	3d3.(2G).4p	1G*	4	213533.9	282037.7	1459.7720		0.0020				1.6e-01	5.95E+09	2667
261	3d3.(4F).4s	3F	3	3d3.(4F).4p	3G*	4	195933.2	264434.2	1459.8330		0.0030				3.0e-01	5.03E+09	2416
262	3d3.(4F).4s	5F	4	3d3.(4F).4p	5G*	4	187719.0	256178.0	1460.7298	★	0.0023	1460.7297	◊	0.0031	6.3e-02	9.52E+08	1771
263	3d3.(2F).4s	3F	3	3d3.(2F).4p	3F*	2	233848.7	302292.5	1461.0540		0.0030	1461.0627		0.01	2.9e-02	4.31E+09	2033
264	3d3.(2D2).4s	3D	3	3d3.(2P).4p	3D*	2	216538.0	284911.0	1462.5641		0.0019				5.3e-04 [†]	5.21E+09	2067
265	3d3.(4F).4s	5F	1	3d3.(4F).4p	5G*	2	186433.8	254803.5	1462.6350	★	0.0030	1462.6246		0.0093	3.2e-01	9.09E+08	1750
266	3d3.(2F).4s	3F	2	3d3.(2F).4p	3F*	3	234027.1	302376.8	1463.0650		0.0030				4.8e-03	4.29E+09	1941
267	3d3.(2H).4s	3H	5	3d3.(2H).4p	3H*	6	216860.2	285195.8	1463.3660		0.0030				1.4e-03	5.81E+09	2647
268	3d3.(4P).4s	3P	2	3d3.(2P).4p	3P*	1	213649.0	281944.8	1464.2202		0.0024				7.3e-03	5.38E+09	851
269	3d3.(4F).4s	3F	4	3d3.(4F).4p	3G*	5	196838.7	265112.8	1464.6850	★	0.0030	1464.6886		0.0038	2.8e-01	4.98E+09	2232
270	3d3.(2F).4s	3F	2	3d3.(2F).4p	3F*	2	234027.1	302292.5	1464.8730		0.0030	1464.8805		0.0038	2.0e-01	4.31E+09	1886
271	3d3.(4F).4s	5F	3	3d3.(4F).4p	5G*	3	187157.6	255399.4	1465.3790		0.0030	1465.3889		0.0093	7.1e-02	9.26E+08	1573
272	3d3.(2H).4s	1H	5	3d3.(2H).4p	1G*	4	221304.9	289546.0	1465.3920		0.0030				1.6e-01	3.56E+09	2945
273	3d3.(2G).4s	3G	4	3d3.(2G).4p	3H*	5	209109.9	277292.5	1466.6498		0.0018	1466.6552		0.0038	1.9e-01	1.68E+09	2212
274	3d3.(2P).4s	3P	2	3d3.(2P).4p	1D*	2	214525.6	282604.8	1468.8770		0.0020				9.0e-03	2.29E+09	2264
275	3d3.(4F).4s	5F	2	3d3.(4F).4p	5G*	2	186725.7	254803.5	1468.9080	★	0.0030	1468.9165		0.0055	6.4e-02	9.09E+08	1420
276	3d3.(2H).4s	3H	6	3d3.(2H).4p	3H*	6	217122.3	285195.8	1469.0000	★	0.0030	1469.0093		0.0055	2.0e-01	5.81E+09	2431
277	3d3.(2P).4s	3P	2	3d3.(2G).4p	1F*	3	214525.6	282571.4	1469.5986		0.0020				1.3e-02	3.61E+09	3313
278	3d3.(2D2).4s	3D	1	3d3.(2P).4p	3D*	1	215782.4	283753.9	1471.2059		0.0020				2.4e-02	5.29E+09	1774
279	3d3.(4F).4s	3F	3	3d3.(4F).4p	3G*	3	195933.2	263898.7	1471.3340		0.0030				1.2e-02	5.05E+09	1754
280	3d3.(2H).4s	3H	5	3d3.(2H).4p	3H*	5	216860.2	284790.5	1472.0980	★	0.0023	1472.1041	◊	0.0026	1.9e-01	5.78E+09	2264
281	3d3.(2H).4s	3H	4	3d3.(2H).4p	3H*	4	216779.1	284690.3	1472.5116	★	0.0024	1472.5158	◊	0.0024	2.0e-01	5.99E+09	2576
282	3d3.(2P).4s	3P	2	3d3.(4P).4p	5S*	2	214525.6	282423.2	1472.8050		0.0018	1472.809		0.0024	2.6e-02	1.35E+09	2349
283	3d3.(2H).4s	3H	5	3d3.(2H).4p	3H*	4	216860.2	284690.3	1474.2722		0.0023	1474.2773		0.0026	1.5e-02	5.99E+09	3111
284	3d3.(4F).4s	5F	5	3d3.(4F).4p	5G*	4	188395.4	256178.0	1475.3050		0.0030				2.0e-03	9.52E+08	1007
285	3d3.(2G).4s	3G	5	3d3.(2G).4p	3H*	5	209523.7	277292.5	1475.6059	★	0.0019	1475.6083	◊	0.0024	5.2e-02	1.68E+09	1800
286	3d3.(4F).4s	5F	4	3d3.(4F).4p	5G*	3	187719.0	255399.4	1477.5340		0.0030				3.7e-03	9.26E+08	938
287	3d3.(2H).4s	3H	6	3d3.(2H).4p	3H*	5	217122.3	284790.5	1477.7992		0.0024				1.4e-02	5.78E+09	2048
288	3d3.(4F).4s	5F	3	3d3.(4F).4p	5G*	2	187157.6	254803.5	1478.2870		0.0030				3.6e-03	9.09E+08	926
289	3d3.(2P).4s	3P	1	3d3.(2P).4p	3P*	0	214611.3	282234.3	1478.7850		0.0030	1478.7865		0.0024	7.8e-02	5.18E+09	2037
290	3d3.(4F).4s	3F	4	3d3.(4F).4p	3G*	4	196838.7	264434.2	1479.3900		0.0030				6.8e-03	5.03E+09	1410
291	3d3.(2G).4s	3G	3	3d3.(2G).4p	3H*	4	208838.0	276429.4	1479.4771		0.0021	1479.4765		0.0038	2.3e-01	1.53E+09	1643
292	3d3.(2P).4s	3P	2	3d3.(2P).4p	3P*	1	214525.6	281944.8	1483.2574		0.0024				1.1e-01	5.38E+09	1555
293	3d3.(2P).4s	1P	1	3d3.(4P).4p	3D*	2	219486.7	286862.5	1484.2120		0.0020				4.0e-02	6.41E+09	1587
294	3d3.(2P).4s	1P	1	3d3.(4P).4p	3D*	1	219486.7	286855.2	1484.3750		0.0021				3.1e-03	6.49E+09	1535
295	3d3.(2D1).4s	1D	2	3d3.(2D1).4p	1D*	2	262509.1	329848.4	1485.0180		0.0040				1.8e-01	5.92E+09	
296	3d3.(2G).4s	3G	4	3d3.(2G).4p	3H*	4	209109.9	276429.4	1485.4533	★	0.0019				4.0e-02	1.53E+09	1418
297	3d3.(2G).4s	1G	4	3d3.(2G).4p	3F*	3	213533.9	280831.9	1485.9263		0.0022				5.9e-03	6.25E+09	3092
298	3d3.(2D2).4s	3D	3	3d3.(2D2).4p	3P*	2	216538.0	283686.1	1489.2434	★	0.0018				5.9e-02	4.67E+09	2589
299	3d3.(2G).4s	3G	5	3d3.(2G).4p	3H*	4	209523.7	276429.4	1494.6412		0.0021				1.5e-03	1.53E+09	1006
300	3d3.(2H).4s	1H	5	3d3.(2H).4p	3I*	6	221304.9	288167.0	1495.6150		0.0030				5.9e-03	1.80E+09	2270
301	3d3.(2G).4s	1G	4	3d3.(2G).4p	3F*	4	213533.9	280366.9	1496.2648	★	0.0023	1496					

Table A1 Continued: Summary of laboratory and Ritz wavelength

ID	C1	T1	J1	C2	T2	J2	E1 (cm^{-1})	E2 (cm^{-1})	K14		W19		f	$\Gamma(\text{s}^{-1})$	$q(\text{cm}^{-1})$
									$\lambda(\text{\AA})$	$\delta\lambda(\text{\AA})$	$\lambda(\text{\AA})$	$\delta\lambda(\text{\AA})$			
311	3d3.(4F).4s	3F	2	3d3.(4F).4p	3D*	3	195196.5	261179.7	1515.5359	0.0024			2.9e-03	3.62E+09	3306
312	3d3.(2P).4s	3P	1	3d3.(2G).4p	3F*	2	214611.3	280539.6	1516.7993	0.0021			2.8e-02	5.92E+09	2965
313	3d3.(2D2).4s	1D	2	3d3.(4P).4p	3D*	3	220620.8	286431.1	1519.5178	0.0021			6.8e-03	5.62E+09	2044
314	3d3.(2D2).4s	1D	2	3d3.(2P).4p	3S*	1	220620.8	286187.5	1525.1631	0.0022			5.0e-03	7.30E+09	2379
315	3d3.(2P).4s	1P	1	3d3.(2P).4p	3D*	2	219486.7	284911.0	1528.4843	0.0021			3.1e-02	5.21E+09	1379
316	3d3.(2D2).4s	1D	2	3d3.(2D2).4p	1P*	1	220620.8	285961.4	1530.4401	0.0023	1530.4446	0.0024	9.1e-02	6.90E+09	2013
317	3d3.(2G).4s	1G	4	3d3.(2G).4p	3G*	3	213533.9	278794.0	1532.3289	0.0023			1.3e-02	7.63E+09	1900
318	3d3.(4F).4s	3F	3	3d3.(4F).4p	3D*	3	195933.2	261179.7	1532.6480	0.0030			2.3e-02	3.62E+09	2462
319	3d3.(4F).4s	3F	2	3d3.(4F).4p	3D*	2	195196.5	260411.6	1533.3870	0.0030			2.2e-02	3.64E+09	2921
320	3d3.(4P).4s	3P	2	3d3.(2G).4p	3G*	3	213649.0	278794.0	1535.0382	0.0023			1.4e-05 [†]	7.63E+09	905
321	3d3.(4F).4s	3F	2	3d3.(4F).4p	5F*	1	195196.5	259995.4	1543.2340	★ 0.0030	1543.2397	△ 0.0024	6.5e-02	3.64E+09	2774
322	3d3.(4F).4s	3F	3	3d3.(4F).4p	3D*	2	195933.2	260411.6	1550.9060	0.0030			8.5e-02	3.64E+09	2077
323	3d3.(4F).4s	3F	4	3d3.(4F).4p	3D*	3	196838.7	261179.7	1554.2180	★ 0.0030			1.3e-01	3.62E+09	1456
324	3d3.(2D2).4s	1D	2	3d3.(2P).4p	3D*	2	220620.8	284911.0	1555.4456	0.0020			2.2e-02	5.21E+09	2074
325	3d3.(4P).4s	3P	0	3d3.(4P).4p	3P*	1	212542.0	276765.8	1557.0542	0.0023			9.5e-02	2.12E+09	3764
326	3d3.(4F).4s	3F	4	3d3.(4F).4p	5F*	5	196838.7	261052.0	1557.3100	0.0030			1.2e-02	3.37E+09	2299
327	3d3.(2P).4s	1P	1	3d3.(2D2).4p	3P*	2	219486.7	283686.1	1557.6467	0.0021			1.9e-02	4.67E+09	1901
328	3d3.(4F).4s	3F	2	3d3.(4F).4p	5F*	2	195196.5	259376.3	1558.1217	0.0023			2.3e-03	6.02E+09	3389
329	3d3.(4F).4s	3F	3	3d3.(4F).4p	5F*	3	195933.2	259955.0	1561.9670	0.0030			9.0e-04	4.95E+09	3532
330	3d3.(4P).4s	3P	1	3d3.(4P).4p	3P*	1	212818.0	276765.8	1563.7745	0.0020			2.2e-02	2.12E+09	3510
331	3d3.(4P).4s	3P	1	3d3.(4P).4p	5D*	2	212818.0	276759.1	1563.9391	0.0020			1.8e-02	1.85E+09	3000
332	3d3.(2G).4s	1G	4	3d3.(2G).4p	3H*	5	213533.9	277292.5	1568.4151	0.0021			4.2e-03	1.68E+09	2607
333	3d3.(4F).4s	3F	2	3d3.(4F).4p	5D*	1	195196.5	258891.5	1569.9810	0.0030			6.9e-03	7.25E+09	2684
334	3d3.(4P).4s	3P	1	3d3.(4P).4p	5D*	0	212818.0	276434.8	1571.9100	★ 0.0030			3.1e-02	2.18E+09	2522
335	3d3.(4F).4s	3F	3	3d3.(4F).4p	5F*	2	195933.2	259376.3	1576.2143	0.0024			9.3e-03	6.02E+09	2545
336	3d3.(2H).4s	3H	5	3d3.(2G).4p	3G*	5	216860.2	280039.5	1582.7979	0.0023			3.6e-03	7.58E+09	2521
337	3d3.(2D2).4s	1D	2	3d3.(2P).4p	3D*	1	220620.8	283753.9	1583.9544	0.0022			2.4e-03	5.29E+09	692
338	3d3.(2P).4s	1P	1	3d3.(2P).4p	1D*	2	219486.7	282604.8	1584.3320	0.0030			8.0e-02	2.29E+09	844
339	3d3.(4P).4s	3P	2	3d3.(4P).4p	3P*	1	213649.0	276765.8	1584.3652	0.0022			2.8e-02	2.12E+09	2507
340	3d3.(4P).4s	3P	2	3d3.(4P).4p	5D*	2	213649.0	276759.1	1584.5342	0.0020			4.8e-02	1.85E+09	1997
341	3d3.(2D2).4s	1D	2	3d3.(2D2).4p	3P*	2	220620.8	283686.1	1585.6560	0.0019			1.5e-02	4.67E+09	2596
342	3d3.(2D2).4s	3D	3	3d3.(2G).4p	3G*	4	216538.0	279502.4	1588.1970	0.0023			4.6e-03	7.46E+09	1740
343	3d3.(2P).4s	1P	1	3d3.(4P).4p	5S*	2	219486.7	282423.2	1588.9028	0.0022			4.6e-02	1.35E+09	929
344	3d3.(4F).4s	3F	2	3d3.(4F).4p	5D*	2	195196.5	258128.7	1589.0110	0.0030			1.2e-02	5.85E+09	1717
345	3d3.(2H).4s	3H	6	3d3.(2G).4p	3G*	5	217122.3	280039.5	1589.3908	0.0024			7.4e-03	7.58E+09	2305
346	3d3.(2G).4s	1G	4	3d3.(2G).4p	3H*	4	213533.9	276429.4	1589.9376	0.0022			8.2e-04	1.53E+09	1813
347	3d3.(4F).4s	3F	3	3d3.(4F).4p	5D*	3	195933.2	258680.1	1593.7032	0.0024			6.5e-03	6.76E+09	1636
348	3d3.(2H).4s	3H	5	3d3.(2G).4p	3G*	4	216860.2	279502.4	1596.3679	0.0022			6.1e-03	7.46E+09	2044
349	3d3.(4P).4s	3P	0	3d3.(4P).4p	5D*	1	212542.0	275146.5	1597.3270	★ 0.0030			9.2e-02	2.09E+09	1802
350	3d3.(4P).4s	3P	1	3d3.(4P).4p	3P*	2	212818.0	275374.1	1598.5639	0.0020			6.2e-02	2.60E+09	1934
351	3d3.(4F).4s	3F	2	3d3.(4F).4p	3D*	1	195196.5	257742.4	1598.8240	★ 0.0030			6.1e-02	4.72E+09	1157
352	3d3.(4F).4s	3F	4	3d3.(4F).4p	5D*	4	196838.7	259345.0	1599.8400	0.0030			1.6e-03	7.52E+09	1485
353	3d3.(4P).4s	5P	3	3d3.(4F).4p	3F*	4	205536.2	267928.5	1602.7610	0.0030			6.8e-04 [†]	5.10E+09	3005
354	3d3.(2P).4s	3P	2	3d3.(4P).4p	3P*	1	214525.6	276765.8	1606.6786	0.0021			3.9e-03	2.12E+09	3211
355	3d3.(4F).4s	3F	3	3d3.(4F).4p	5D*	2	195933.2	258128.7	1607.8330	★ 0.0030			3.7e-02	5.85E+09	873
356	3d3.(2D2).4s	1D	2	3d3.(2G).4p	1F*	3	220620.8	282571.4	1614.1888	0.0023			3.6e-02	3.61E+09	2588
357	3d3.(4F).4s	3F	4	3d3.(4F).4p	5D*	3	196838.7	258680.1	1617.0400	0.0030			1.6e-02	6.76E+09	630
358	3d3.(2D2).4s	1D	2	3d3.(4P).4p	5S*	2	220620.8	282423.2	1618.0580	0.0021			1.3e-02	1.35E+09	1624
359	3d3.(2H).4s	3H	5	3d3.(2G).4p	3H*	6	216860.2	278650.5	1618.3790	0.0030			1.6e-03	1.43E+09	3209
360	3d3.(4P).4s	3P	2	3d3.(4P).4p	3P*	2	213649.0	275374.1	1620.0873	0.0020			9.3e-02	2.60E+09	931
361	3d3.(2H).4s	1H	5	3d3.(2G).4p	1H*	5	221304.9	282871.6	1624.2550	★ 0.0030			4.8e-02	2.37E+09	2023
362	3d3.(2H).4s	3H	6	3d3.(2G).4p	3H*	6	217122.3	278650.5	1625.2720	★ 0.0030			5.8e-02	1.43E+09	2993
363	3d3.(4P).4s	3P	2	3d3.(4P).4p	5D*	1	213649.0	275146.5	1626.0826	0.0022			2.2e-02	2.09E+09	545
364	3d3.(4P).4s	3P	1	3d3.(4P).4p	5P*	2	212818.0	274135.9	1630.8433	0.0022			3.7e-03	6.76E+09	2641
365	3d3.(2D2).4s	3D	1	3d3.(4P).4p	3P*	1	215782.4	276765.8	1639.7918	0.0022			3.3e-03	2.12E+09	3568
366	3d3.(2P).4s	3P	2	3d3.(4P).4p	3P*	2	214525.6	275374.1	1643.4256	0.0021			1.1e-03	2.60E+09	1635
367	3d3.(2P).4s	3P	1	3d3.(4P).4p	3P*	2	214611.3	275374.1	1645.7430	0.0021			1.0e-02	2.60E+09	1515
368	3d3.(2D2).4s	3D	1	3d3.(4P).4p	5D*	0	215782.4	276434.8	1648.7400	0.0030			5.7e-03	2.18E+09	2580
369	3d3.(2P).4s	3P	1	3d3.(4P).4p	5D*	1	214611.3	275146.5	1651.9301	0.0023			6.6e-03	2.09E+09	1129
370	3d3.(2H).4s	3H	4	3d3.(2G).4p	3H*	5	216779.1	277292.5	1652.5280	0.0020			2.1e-03	1.68E+09	1353
371	3d3.(4P).4s	3P	2	3d3.(4P).4p	5P*	2	213649.0	274135.9	1653.2508	0.0022			1.1e-02	6.76E+09	1638
372	3d3.(2H).4s	3H	5	3d3.(2G).4p	3H*	5	216860.2	277292.5	1654.7456	★ 0.0021			4.0e-02	1.68E+09	1888
373	3d3.(4F).4s	3F	3	3d3.(4F).4p	5G*	4	195933.2	256178.0	1659.8940	0.0030			2.9e-03	9.52E+08	1870
374	3d3.(2D2).4s	3D	3	3d3.(4P).4p	5D*</td										

Table A1 Continued: Summary of laboratory and Ritz wavelength

ID	C1		T1		J1		C2		T2		J2		E1 (cm ⁻¹)	E2 (cm ⁻¹)	K14		W19		f	Γ (s ⁻¹)	q (cm ⁻¹)
															λ (Å)	$\delta\lambda$ (Å)	λ (Å)	$\delta\lambda$ (Å)			
378	3d3.(2D2).4s	1D	2	3d3.(2G).4p	3F*	2	220620.8	280539.6	1668.9250	0.0024									4.8e-03	5.92E+09	2360
379	3d3.(2H).4s	3H	4	3d3.(2G).4p	3H*	4	216779.1	276429.4	1676.4380	★	0.0030								3.5e-02	1.53E+09	559
380	3d3.(2H).4s	3H	5	3d3.(2G).4p	3H*	4	216860.2	276429.4	1678.7207	0.0024									1.1e-03	1.53E+09	1094
381	3d3.(2D2).4s	3D	3	3d3.(4P).4p	3P*	2	216538.0	275374.1	1699.6353	0.0023									8.6e-03	2.60E+09	903
382	3d3.(2F).4s	3F	4	3d3.(2H).4p	3G*	5	233633.5	292287.3	1704.9180	0.0030									1.6e-02	8.20E+09	3264

A2 Observed lines

Table A2: Observed line wavelengths in the STIS spectrum of G191-B2B. ID refers to the number in column 1 of Table A1. λ_{obs} is the mean observed-frame wavelength of the absorption feature with uncertainty $\sigma(\lambda_{\text{obs}})$. EW is the equivalent width with uncertainty $\sigma(\text{EW})$. The absence of $\sigma(\text{EW})$ indicates that another line is nearby such that the detection algorithm interpreted the whole feature as a blend. Wavelength and equivalent widths are in Å. Columns 6-11 give redshift z, b-parameter (in km/s) and column density logN (N is in atoms/cm) with their associated uncertainties. A tick in the last two columns indicates that a line was used for measuring α .

ID	λ_{obs}	$\sigma(\lambda_{\text{obs}})$	EW	$\sigma(\text{EW})$	z	[$\times 10^{-5}$]	$\sigma(z)$ [$\times 10^{-5}$]	b	$\sigma(b)$	logN	$\sigma(\text{logN})$	K14	W19
27	1250.833	0.001	0.003		7.88	0.06	4.99	0.30	12.12	0.02	✓		
36	1280.573	0.0012	0.00617	0.000197	8.17	0.04	5.36	0.18	13.22	0.01	✓	✓	
38	1281.468	0.001	0.002		7.93	0.11	5.11	0.59	12.15	0.04	✓		
43	1286.015	0.001	0.002		7.73	0.06	3.68	0.30	12.51	0.02	✓	✓	
45	1288.269	0.0009	0.00355	0.000148	7.89	0.04	3.98	0.20	12.73	0.01	✓	✓	
48	1291.298	0.002	0.005		8.24	0.07	6.50	0.30	12.90	0.02	✓	✓	
50	1293.409	0.001	0.003		7.85	0.06	5.47	0.27	13.09	0.02	✓		
51	1293.485	0.001	0.003		7.92	0.04	4.40	0.18	12.85	0.01	✓		
52	1297.651	0.001	0.005		7.95	0.04	5.13	0.17	12.91	0.01	✓	✓	
53	1300.715	0.001	0.0047	0.000162	8.09	0.04	4.59	0.18	12.90	0.01	✓		
61	1307.531	0.0007	0.00656	0.00017	8.12	0.03	5.04	0.15	12.33	0.01	✓	✓	
65	1311.934	0.0008	0.00528	0.000163	7.97	0.03	4.14	0.16	12.29	0.01	✓	✓	
66	1313.698	0.002	0.002		8.48	0.12	5.89	0.56	12.24	0.03	✓		
67	1314.634	0.0013	0.00371	0.000184	8.22	0.05	5.27	0.25	14.06	0.01	✓	✓	
75	1321.957	0.001	0.003		8.08	0.06	4.99	0.31	12.99	0.02	✓	✓	
77	1323.376	0.001	0.013		8.03	0.02	5.24	0.08	12.74	0.00			
79	1325.885	0.003	0.004		7.72	0.06	5.16	0.29	13.10	0.02	✓	✓	
83	1331.286	0.0022	0.00289	0.000263	7.51	0.10	4.33	0.47	12.40	0.03	✓		
84	1331.745	0.0012	0.0076	0.000292	7.93	0.04	4.56	0.18	12.51	0.01	✓	✓	
88	1338.911	0.0016	0.00289	0.000208	7.78	0.07	4.25	0.35	12.83	0.02	✓		
89	1339.792	0.001	0.006		7.55	0.07	5.81	0.33	12.42	0.02	✓		
93	1350.639	0.0012	0.00421	0.000226	7.54	0.07	3.94	0.35	12.35	0.02	✓		
104	1358.67	0.002	0.003		7.86	0.10	4.66	0.49	12.41	0.03	✓	✓	
109	1361.548	0.0009	0.00896	0.000258	7.69	0.03	4.95	0.17	12.32	0.01	✓	✓	
111	1361.932	0.001	0.01258	0.000301	7.58	0.03	5.55	0.13	12.43	0.01	✓	✓	
116	1364.922	0.001	0.006		7.62	0.05	5.44	0.23	12.96	0.01	✓		
123	1370.418	0.0021	0.0021	0.000225	8.29	0.13	4.62	0.66	13.01	0.05	✓	✓	
124	1371.047	0.001	0.00626	0.000243	7.67	0.04	4.21	0.21	12.67	0.01	✓	✓	
126	1372.095	0.001	0.00507	0.000233	8.00	0.07	4.78	0.32	12.37	0.02	✓	✓	
128	1373.695	0.02			7.90	0.02	5.92	0.07	12.85	0.00	✓		
129	1373.784	0.001	0.018		7.51	0.02	5.44	0.09	12.78	0.01	✓		
130	1374.072	0.0011	0.00845	0.000282	7.77	0.03	5.42	0.18	12.58	0.01	✓	✓	
131	1374.223	0.0007	0.00983	0.000268	7.62	0.03	4.86	0.12	12.30	0.01	✓	✓	
136	1376.444	0.001	0.023		7.98	0.02	5.98	0.08	12.86	0.00			
137	1376.563	0.001	0.014		8.13	0.02	5.26	0.11	12.71	0.01			
140	1378.666	0.001	0.017		7.64	0.03	5.43	0.12	12.53	0.01	✓	✓	
142	1380.219	0.001	0.0112	0.000309	7.58	0.03	4.99	0.16	12.58	0.01	✓	✓	
149	1385.424	0.001	0.006		8.09	0.05	4.69	0.24	12.65	0.01	✓	✓	
156	1388.141	0.0038	0.00145	0.000283	7.26	0.17	3.01	0.89	12.81	0.08	✓		
157	1388.305	0.001	0.004		7.78	0.11	4.95	0.56	12.38	0.04	✓	✓	
158	1388.435	0.001	0.008		8.19	0.13	4.74	0.49	12.40	0.04	✓	✓	
165	1393.179	0.0012	0.00588	0.000291	7.92	0.09	4.74	0.42	12.70	0.03	✓	✓	
166	1394.383	0.0012	0.00913	0.000332	8.05	0.04	4.98	0.19	12.74	0.01	✓		
170	1397.219	0.0015	0.00367	0.000281	7.58	0.12	4.14	0.59	12.29	0.04	✓	✓	
171	1397.861	0.002	0.002		7.61	0.19	4.22	0.95	12.37	0.07	✓		
172	1398.078	0.002	0.007		7.74	0.06	5.49	0.28	12.83	0.02	✓	✓	
174	1400.355	0.0009	0.01443	0.000342	8.62	0.06	4.74	0.24	12.57	0.02	✓		
181	1404.377	0.0015	0.00254	0.000233	8.30	0.15	4.19	0.73	11.95	0.05	✓	✓	

Table A2 Continued:

ID	λ_{obs}	$\sigma(\lambda_{\text{obs}})$	EW	$\sigma(\text{EW})$	z [$\times 10^{-5}$]	$\sigma(z)$ [$\times 10^{-5}$]	b	$\sigma(b)$	logN	$\sigma(\text{logN})$	K14	W19
185	1407.357	0.0007	0.01707	0.000327	7.80	0.04	5.50	0.16	12.55	0.01	✓	✓
187	1408.235	0.0008	0.00851	0.000281	8.04	0.06	4.40	0.26	12.83	0.02	✓	✓
188	1408.906	0.002	0.002		7.83	0.22	4.89	1.04	12.93	0.06	✓	
190	1409.337	0.0008	0.01824	0.000356	8.09	0.03	5.40	0.15	12.83	0.01	✓	
193	1409.962	0.0009	0.00833	0.000272	8.01	0.04	4.69	0.20	12.92	0.01	✓	
195	1411.68	0.001	0.01		7.90	0.05	5.51	0.21	12.94	0.01	✓	✓
196	1414.946	0.0015	0.00333	0.000229	8.19	0.08	3.16	0.38	12.81	0.03	✓	
199	1416.336	0.001	0.009		8.12	0.06	4.79	0.26	12.33	0.02	✓	✓
205	1420.532	0.001	0.004		7.89	0.09	3.90	0.47	12.95	0.04	✓	
206	1420.591	0.001	0.005		7.94	0.08	4.44	0.42	12.59	0.03	✓	
207	1420.714	0.001	0.011		7.71	0.04	4.89	0.20	12.73	0.01	✓	✓
209	1421.126	0.003	0.00279	0.000324	7.70	0.10	4.02	0.50	12.29	0.04	✓	
211	1422.594	0.0011	0.00487	0.000269	7.99	0.07	3.78	0.31	12.27	0.02	✓	✓
213	1425.201	0.003	0.002		8.08	0.16	3.89	0.75	12.67	0.05	✓	✓
220	1430.421	0.0024	0.00452	0.000454	7.44	0.11	3.78	0.51	12.26	0.04	✓	
222	1430.865	0.001	0.005		7.67	0.10	3.56	0.50	12.63	0.04	✓	
226	1435.156	0.0015	0.0075	0.000441	7.50	0.07	4.70	0.35	12.97	0.02	✓	
229	1440.642	0.001	0.021		7.79	0.02	5.51	0.11	12.71	0.01	✓	✓
230	1440.906	0.0016	0.00636	0.000369	7.72	0.07	4.82	0.35	12.40	0.02	✓	✓
241	1448.605	0.0011	0.01005	0.00037	8.14	0.05	4.82	0.25	12.62	0.02	✓	
244	1450.036	0.001	0.01		7.42	0.05	4.78	0.23	12.40	0.02	✓	✓
245	1451.211	0.003	0.002		7.92	0.24	5.30	1.11	12.41	0.06	✓	✓
250	1453.739	0.001	0.015		8.23	0.03	5.85	0.18	12.66	0.01	✓	✓
253	1454.808	0.0014	0.00896	0.000421	7.49	0.07	5.06	0.34	13.09	0.02	✓	✓
254	1455.674	0.0012	0.01661	0.000486	8.13	0.03	5.54	0.15	12.48	0.01	✓	✓
256	1456.28	0.001	0.017		7.97	0.04	5.61	0.16	12.62	0.01	✓	✓
257	1456.4	0.002	0.008		7.62	0.07	4.95	0.31	12.59	0.02	✓	✓
259	1459.363	0.0018	0.00848	0.000406	7.67	0.06	5.64	0.25	12.35	0.01	✓	✓
262	1460.846	0.0014	0.01082	0.000459	7.83	0.05	4.64	0.21	12.99	0.01	✓	✓
265	1462.751	0.001	0.015		7.83	0.04	5.26	0.20	12.45	0.01	✓	
269	1464.798	0.001	0.021		7.73	0.03	5.89	0.14	12.67	0.01	✓	
275	1469.026	0.001	0.009		8.07	0.08	5.75	0.35	12.92	0.02	✓	
276	1469.12	0.001	0.015		8.11	0.04	5.06	0.20	12.65	0.01	✓	
280	1472.217	0.001	0.013		8.07	0.04	4.99	0.18	12.60	0.01	✓	✓
281	1472.633	0.001	0.012		8.07	0.05	4.92	0.23	12.54	0.01	✓	✓
285	1475.718	0.002	0.00672	0.000438	7.81	0.11	5.17	0.50	12.84	0.03	✓	✓
296	1485.573	0.0022	0.00535	0.000433	7.93	0.12	5.42	0.56	12.86	0.03	✓	
298	1489.357	0.0021	0.00475	0.0004	7.56	0.10	4.24	0.48	12.64	0.03	✓	
301	1496.382	0.001	0.008		7.97	0.08	4.61	0.39	12.69	0.03	✓	✓
321	1543.363	0.0015	0.0043	0.000374	8.41	0.07	2.80	0.38	12.53	0.04	✓	✓
323	1554.346	0.0015	0.01213	0.000557	8.27	0.05	5.10	0.24	12.70	0.01	✓	
334	1572.042	0.004	0.002	0.001	8.25	0.36	4.50	1.66	12.57	0.11	✓	
349	1597.449	0.0043	0.00305	0.000543	9.13	0.64	10.91	2.78	12.36	0.09	✓	
351	1598.956	0.0035	0.00396	0.000612	8.25	0.21	4.61	1.04	12.56	0.08	✓	
355	1607.966	0.003	0.005	0.001	7.90	0.26	7.85	1.15	12.96	0.05	✓	
361	1624.388	0.0043	0.00288	0.000664	8.74	0.34	4.32	1.69	12.38	0.13	✓	
362	1625.399	0.0026	0.00711	0.000731	7.79	0.12	3.44	0.61	12.78	0.05	✓	
372	1654.881	0.003	0.004	0.001	8.42	0.11	2.02	0.58	12.63	0.06	✓	
379	1676.572	0.003	0.003		8.30	0.25	4.16	1.17	12.69	0.09	✓	

This paper has been typeset from a T_EX/L_AT_EX file prepared by the author.